Somatic mosaicism in amyotrophic lateral sclerosis and frontotemporal dementia identifies focal mutations associated with widespread degeneration

Zinan Zhou[1,2,3,12], Junho Kim[1,2,3,4,12], August Yue Huang[1,2,3,12], Matthew Nolan[5], Junseok Park[1,2,3], Ryan Doan[1,3], Taehwan Shin[1,2,3], Michael B. Miller[1,6], Mingyun Bae[1,2,3], Boxun Zhao[1,2,3], Jinhyeong Kim[4], Brian Chhouk[1,2,3], Katherine Morillo[1,2,3], Rebecca C. Yeh[1,2,3], Connor Kenny[1,2,3], Jennifer E. Neil[1,2,3,7], Chao-Zong Lee[5], Takuya Ohkubo[8,9], John Ravits[9], Olaf Ansorge[10], Lyle W. Ostrow[11], Clotilde Lagier-Tourenne[5,13], Eunjung Alice Lee[1,2,3,13] and Christopher A. Walsh[1,2,3,7,13]

Affiliations

[1]Division of Genetics and Genomics, Boston Children's Hospital, Boston, MA, USA.
[2]Manton Center for Orphan Disease, Boston Children's Hospital, Boston, MA, USA.
[3]Department of Pediatrics, Harvard Medical School, Boston, MA, USA.
[4]Department of Biological Sciences, Sungkyunkwan University, Suwon, South Korea.
[5]Department of Neurology, The Sean M. Healey and AMG Center for ALS at Mass General, Massachusetts General Hospital, Harvard Medical School, Boston, MA, USA.
[6]Department of Pathology, Brigham and Women's Hospital, Harvard Medical School, Boston, MA, USA.
[7]Howard Hughes Medical Institute, Boston Children's Hospital, Boston, MA, USA.
[8]Department of Neurology, Yokohama City Minato Red Cross Hospital, Yokohama, Kanagawa, Japan.
[9]Department of Neurosciences, School of Medicine, University of California San Diego, La Jolla, CA, USA.
[10]Nuffield Department of Clinical Neurosciences, University of Oxford, Oxford, Oxfordshire, UK.
[11]Department of Neurology, Lewis Katz School of Medicine at Temple University, Philadelphia, PA, USA.
[12]These authors contributed equally: Zinan Zhou, Junho Kim, August Yue Huang.
[13]These authors jointly supervised this work: Clotilde Lagier-Tourenne, Eunjung Alice Lee, Christopher A. Walsh. e-mail: clagier-tourenne@mgh.harvard.edu; ealee@childrens.harvard.edu; christopher.walsh@childrens.harvard.edu.

Abstract

Although mutations in many genes cause familial amyotrophic lateral sclerosis and frontotemporal dementia, most cases are sporadic (sALS and sFTD) with unclear etiology. We tested whether somatic mutations contribute to sALS and sFTD by deep targeted sequencing of 88 neurodegeneration-related genes in postmortem brain and spinal cord samples from 399 sporadic cases and 144 controls. Predicted deleterious somatic variants in ALS/FTD genes were observed in 2.1% of sporadic cases lacking deleterious germline variants. These variants occurred at very low allele fractions (typically <2%) and were often focal and enriched in disease-affected regions. Analysis of bulk RNA-seq data from an additional cohort identified deleterious somatic variants in *DYNC1H1* and *LMNA*, genes associated with pediatric motor neuron degeneration. Targeted long-read sequencing further identified one sFTD case with *de novo* somatic *C9orf72* repeat expansions. Together, these findings suggest that rare, focal somatic variants can contribute to sALS and sFTD and drive widespread neurodegeneration.

Introduction

Amyotrophic lateral sclerosis (ALS), a disease in which premature loss of upper and lower motor neurons (UMNs and LMNs) leads to fatal paralysis, shows clinical, genetic, and pathological overlap with frontotemporal dementia (FTD), a neurodegenerative disorder characterized by behavioral, language, and memory dysfunction[1]. 5-22% of individuals with ALS develop FTD, and ~15% of those with FTD eventually develop ALS[2]. ALS and FTD also share common pathology, with cytoplasmic inclusions of TAR DNA binding protein (TDP-43) found in almost all ALS brains and in half of FTD brains[3,4]. ALS typically begins focally and spreads regionally as the disease progresses[5,6], although whether degeneration begins in UMNs, LMNs, or both simultaneously has remained controversial[7,8], with some studies suggesting that focality can manifest independently in UMNs and LMNs[5,9]. TDP-43 pathology also follows stereotypical patterns in ALS and FTD brains[9-11], thought to reflect focal onset and intercellular transmission of TDP-43 inclusions in a prion-like manner, as shown in cell and animal models[12-18].

Whereas over 30 genes are implicated in ALS and FTD[19], most causative genes are linked to familial ALS (fALS) and FTD (fFTD), while 90-95% of cases are sporadic ALS (sALS) and FTD (sFTD) without a family history[20]. The focal onset of ALS and FTD, their stereotypical spread, and the increased risk in smokers[21] have raised interest in potential roles of somatic mosaic mutations in the pathogenesis of ALS and FTD[22]. Somatic mutations are increasingly recognized as prevalent in normal-appearing tissues, but somatic mutations responsible for neurological conditions are often limited to the central nervous system (CNS)[23], and hence undetectable through DNA sequencing of non-CNS tissues. Recent studies have evaluated the contributions of somatic mutation to Alzheimer's and Parkinson's disease directly using postmortem brain tissues[24].

In this study, we assessed potential contributions of somatic variants—distinguished by their variant allele frequencies (VAFs)—to sALS and sFTD using deep sequencing of a panel of neurodegeneration/dementia-associated genes on postmortem tissues of various brain regions and spinal cords from 399 unique sALS and sFTD cases. Our study identified novel predicted deleterious somatic variants in 2.1% of the sALS and sFTD cases without pathogenic or predicted deleterious germline variants. Protein-altering (missense/nonsense/frameshift) somatic variants showed enrichment in sALS and sFTD cases and in disease-affected brain regions, supporting roles in disease pathogenesis. Regional analysis revealed focality of predicted deleterious somatic variants in primary motor cortex and spinal cord, supporting independent disease initiation in UMNs and LMNs, but also strongly supporting models of ALS and FTD in which the disease spreads beyond a relatively confined region containing a somatic variant. Complementary analyses of bulk RNA-seq and targeted long-read sequencing of brain and spinal cord tissues further revealed somatic variants in genes not previously associated with ALS or FTD, as well as a *de novo* somatic *C9orf72* repeat expansion. Together, our study opens new avenues for understanding the etiology of sporadic ALS and FTD.

Results

Deep targeted sequencing of neurodegenerative genes in sALS and sFTD brains

To directly detect somatic variants in sALS and sFTD brains, we obtained post-mortem frozen tissues of several brain regions and spinal cords from individuals diagnosed with sALS or sFTD, as well as from age-matched controls through the Massachusetts Alzheimer's Disease Research Center, Oxford Brain Bank, and Target ALS Foundation (Fig. 1a and Supplementary Table 1). Additional brain tissues from ALS, FTD and control cases, without a record of family history but

with an age of death above 45 years old, were also obtained from the NIH NeuroBioBank. We performed molecular inversion probe (MIP)-panel sequencing[25] of 88 neurodegeneration-associated genes at ~1,800× deduplicated depth across 1,787 samples from 291 ALS, 117 FTD, and 144 neurotypical control individuals (Fig. 1a,b, Supplementary Fig. 1, Supplementary Table 2, and Supplementary Note).

Pathogenic germline variants in sALS and sFTD cases

We first identified pathogenic germline single-nucleotide variants (SNVs) and short insertions and deletions (indels) using GATK followed by stringent filtering (Fig. 1d), with functional annotation and deleteriousness prediction performed using ANNOVAR[26] and multiple clinical databases. In addition, *C9orf72* repeat expansions, the most common inherited cause of ALS and FTD[27,28], were genotyped by a repeat-primed PCR assay (Supplementary Fig. 2). Overall, 20.6% (60/291) of ALS, 25.6% (30/117) of FTD and 0.7% (1/144) of control cases carried *C9orf72* repeat expansions or pathogenic germline mutations in ALS and FTD genes (Fig. 2a and Supplementary Tables 3 and 4). Missense variants represented the most prevalent variant type (Fig. 2b). *C9orf72* was the most frequently mutated gene, followed by *SOD1* in ALS, and *GRN* and *MAPT* in FTD (Fig. 2c,d). The overall fractions of *C9orf72* repeat expansion carriers (10.6% in ALS; 12.0% in FTD) were slightly higher than previously reported in sporadic cases, but still lower than in familial cases[29-31].

In addition, predicted deleterious germline variants in dominant ALS/FTD genes were found in an additional 14.1% of ALS, 18.8% of FTD, and 4.9% of control cases with significant enrichment observed in both ALS (OR = 3.20, 95% CI: 1.37-8.69, $P = 3.2 \times 10^{-3}$) and FTD (OR = 4.51, 95% CI: 1.77-13.01, $P = 5.5 \times 10^{-4}$) cases (Fig. 2a and Supplementary Tables 3 and 4). While most predicted deleterious variants were non-synonymous SNVs requiring functional validation, two novel *GRN* frameshift variants (p.L46Rfs*18 and p.D250Tfs*6) identified in FTD cases were probably pathogenic (Supplementary Table 3), since loss-of-function *GRN* mutations are known to cause FTD in a dominant manner[32,33]. Consistent with previous reports, we found evidence of possible oligogenic inheritance. This includes one case carrying both *C9orf72* expansion and a pathogenic variant in *ANXA11*, as well as 12 additional cases carrying combinations of pathogenic and predicted deleterious variants (Fig. 2d and Supplementary Table 3)[34-37]. Interestingly, we also identified cross-disease—variants in ALS genes in FTD and vice versa—highlighting potential shared genetic mechanisms (Fig. 2d).

Identification of somatic SNVs and indels from MIP sequencing data

We developed a custom pipeline integrating RePlow[38], Mutect2[39], and Pisces[40] for calling somatic SNVs and indels in our MIP sequencing data (Fig. 1d). We selected somatic variants identified by at least two of the three callers (double-called variants) followed by multi-step variant filters to remove false positive candidates. Unlike heterozygous germline variants with VAFs around 50%, heterozygous somatic variants have VAFs less than 50%, and we only called somatic variants with VAFs below 35%. To benchmark our pipeline, we performed spike-in experiments by mixing two human samples from the Genome in a Bottle Consortium (GIAB) at low VAFs and observed high sensitivity and precision with a low false positive rate across VAFs (Extended Data Fig. 1a,b and Supplementary Note).

We applied our custom pipeline to 1,787 samples to obtain initial somatic variant candidates. Among these, we identified and removed candidates arising from potential sample contamination in 29 samples (Supplementary Note). The remaining call set contained 98 unique

140 somatic SNV and indel candidates (a total of 149 candidates, including shared ones observed in
141 multiple regions of the same individuals; see Supplementary Table 5). Variants with low VAFs
142 (<5%) were more common in disease cases than in normal controls (Extended Data Fig. 2). All
143 somatic candidates were validated by deep amplicon sequencing, except one for which primers
144 could not be designed; 34 exonic candidates were additionally assessed by droplet digital PCR
145 (ddPCR). Thirteen candidates were actually germline variants, consistent with known VAF
146 deviation in MIPs sequencing due to probe hybridization and amplicon design biases[41,42]. After
147 excluding these, 64 out of 85 candidates (75.2%) were validated as somatic (Supplementary
148 Table 6). The VAFs of validated candidates in amplicon sequencing showed a strong correlation
149 with their original VAFs in the MIP sequencing data (Fig. 3a). All subsequent somatic variant
150 analyses were conducted using only the validated candidates.
151
152 **Somatic variants in disease-relevant genes are enriched in ALS and FTD cases lacking**
153 **pathogenic germline variants**
154 To examine the burden and potential roles of somatic variants in ALS and FTD, we focused on
155 cases lacking pathogenic or predicted deleterious germline variants in ALS/FTD genes
156 (germline-free cases), including cases with heterozygous germline variants in recessive
157 ALS/FTD genes (e.g., *ATP13A2*, *ALS2*) that were predicted to be deleterious. Fifty-five unique
158 somatic variants across the targeted regions were identified among 696, 243, and 516 samples
159 from 216 germline-free ALS cases, 78 germline-free FTD cases, and 144 neurotypical controls,
160 respectively. Most of them (78.2%, 43/55) were focal to a single tissue region and present at very
161 low VAFs (Fig. 3b and Extended Data Fig. 2), consistent with late-arising[43], CNS-restricted
162 events. Mutational signature analysis [44] revealed predominance of clock-like signatures (SBS5
163 and SBS1) (Extended Data Fig. 3), consistent with previous studies of somatic mutagenesis in
164 the normal human brain[45,46].
165 Across all targeted neurodegeneration/dementia-related genes, protein-altering somatic
166 variants showed clear separation between disease and control groups (Fig. 3c), with only one
167 such variant observed in controls compared with 15 in ALS and 7 in FTD cases. Both exonic and
168 protein-altering somatic variants were significantly enriched in ALS and FTD (Fig. 4a; exonic: P
169 $= 0.044$ and $P = 0.0014$; protein-altering: $P = 0.019$ and $P = 0.010$; linear mixed model; see
170 Supplementary Note), whereas intronic and non-coding somatic variants showed no enrichment.
171 Consistently, ratios of non-synonymous to non-coding variants were increased in ALS and FTD
172 at both group and individual levels (Extended Data Fig. 4), indicating disease-specific
173 accumulation of potentially damaging variants.
174 When restricted to ALS/FTD genes, exonic and protein-altering variants in established
175 ALS genes were specifically enriched in germline-free ALS cases (Fig. 4b; exonic: $P = 0.046$;
176 protein-altering: $P = 0.026$; linear mixed model). In contrast, germline-free FTD cases showed
177 no enrichment in known FTD genes but exhibited significant enrichment in other
178 neurodegeneration/dementia-related genes (Fig. 4a,b and Extended Data Fig. 5), consistent with
179 broader pathological heterogeneity of FTD, and perhaps implicating a shared genetic architecture
180 with other neurodegenerative diseases. No protein-altering variants in ALS/FTD genes were
181 observed in controls or in ALS/FTD cases carrying pathogenic germline variants (Supplementary
182 Tables 6 and 7).
183 Somatic variants also exhibited region-specific enrichment in disease-affected regions of
184 germline-free ALS and FTD cases (Fig. 4c and Extended Data Fig. 6). Across all targeted genes,
185 enrichment was observed in the primary motor cortex in ALS cases (Extended Data Fig. 6; all: P

186 = 0.020; exonic: $P = 0.026$; protein-altering: $P = 0.012$; linear mixed model) and in the prefrontal
187 cortex of FTD brains (Extended Data Fig. 6; exonic: $P = 2.3 \times 10^{-3}$; protein-altering: $P = 7.7 \times$
188 10^{-4}; linear mixed model). In contrast, the premotor cortex—located immediately between the
189 primary motor cortex and prefrontal cortex—showed no enrichment for either condition. When
190 restricted to ALS/FTD genes, ALS cases still demonstrated the enrichment only in the primary
191 motor cortex (Fig. 4c; all: $P = 8.3 \times 10^{-3}$; exonic: $P = 0.060$; protein-altering: $P = 0.029$; linear
192 mixed model), while FTD cases showed no significant enrichment in the prefrontal cortex,
193 further supporting a broader genetic heterogeneity in FTD. The spinal cord in ALS showed a
194 modest increase in exonic and protein-altering variants, although this analysis is limited by the
195 small number of control samples and wide confidence intervals (Fig. 4c). Together, these
196 diagnosis- and region-specific patterns suggest that functional somatic variants may contribute to
197 the pathogenesis of sALS and sFTD.
198
199 **Predicted deleterious somatic variants have restricted regional distributions and are**
200 **enriched in hypodiploid cells**
201 Pathogenicity prediction identified six predicted deleterious somatic SNVs in known ALS and
202 FTD genes (Supplementary Table 7), which account for 2.3% and 1.3% of germline-free ALS
203 and FTD cases, respectively (2.1% for overall). All variants in ALS cases were observed in
204 primary motor cortex or spinal cord, the most severely affected regions in ALS, emphasizing
205 remarkable topographic specificity. All somatic variants occurred in disease genes with dominant
206 inheritance when found in the germline setting, except for one sALS case with a predicted
207 deleterious somatic *ALS2* (p.T787R) variant identified in the spinal cord. *ALS2* is an autosomal
208 recessive disease gene[47,48], and this individual also carried a predicted deleterious germline *ALS2*
209 (p.Q24R) variant in addition to the identified somatic variant. Both *ALS2* variants were predicted
210 to be deleterious, consistent with a "second hit" mechanism at the cellular level in a small
211 proportion of spinal cord cells.
212 We selected four predicted deleterious somatic SNVs—*TIA1* (p.H54R), *MATR3*
213 (p.K594I), *ALS2* (p.T787R), and *TARDBP* (p.L248F)—for detailed analysis of regional and cell-
214 type distributions. Amplicon sequencing across multiple CNS regions showed that *MATR3*
215 (p.K594I) and *TARDBP* (p.L248F) were restricted to the primary motor cortex (Fig. 4d and
216 Supplementary Table 8), whereas *TIA1* (p.H54R) and *ALS2* (p.T787R) exhibited their highest
217 VAFs in the spinal cord (2.16% and 0.97%, respectively), where they were originally identified,
218 and were detected at much lower levels in other brain regions (Fig. 4d and Supplementary Table
219 8). All four somatic SNVs were absent from the cerebellum. The ultra-low VAFs and focal
220 distribution of these variants suggest that they probably arose late in development and were thus
221 likely CNS-restricted. Together with the enrichment of exonic and protein-altering somatic
222 variants in disease-affected tissue regions, these findings also support the focal onset of ALS at
223 the genetic level in these sporadic cases. Cells carrying damaging somatic variants could form
224 initial lesions, likely TDP-43 inclusions, in UMNs and LMNs, with pathology ultimately
225 spreading to other regions of the motor system that lack or carry exceedingly low levels of the
226 variant, but nonetheless show robust post-mortem pathology otherwise indistinguishable from
227 germline cases. Consistent with this hypothesis, the case harboring the *TARDBP* (p.L248F)
228 variant, showed the highest phospho-TDP-43 (pTDP-43) level in the primary motor cortex,
229 where the variant was detected (Extended Data Fig. 7). Quantification across seven brain regions
230 revealed significant regional differences in pTDP-43 levels ($F = 3.20$, $P = 0.0099$, one-way
231 ANOVA), with the motor cortex exhibiting significantly higher pathology compared to the

232 hippocampus (P = 0.0042), middle temporal gyrus (P = 0.040), and occipital cortex (P = 0.032)
233 in post hoc Tukey's HSD tests. These results support the idea that focal somatic variants may
234 initiate pathology that later spreads to broader brain regions.
235 We then assessed the distribution of these four somatic SNVs across cell types by
236 performing amplicon sequencing of DNA from neuronal (NeuN+), glial (NeuN-), diploid,
237 polyploid, and hypodiploid nuclei isolated by fluorescence-activated nuclei sorting (FANS) from
238 the regions in which the variants were originally identified (Extended Data Fig. 8a,b).
239 Interestingly, *TIA1* (p.H54R), *MATR3* (p.K594I), and *ALS2* (p.T787R) were enriched in
240 hypodiploid nuclei (Extended Data Fig. 8c), which likely represent apoptotic cells
241 (Supplementary Note)[49-52], suggesting a potential association with cell death. Surprisingly, these
242 three variants were identified in all cell fractions, but were more enriched in non-neuronal than
243 neuronal populations (Extended Data Fig. 8c,d). This finding could imply that neurons may
244 exhibit a cell-type-specific vulnerability to damaging somatic variants in ALS/FTD genes.
245 However, further research is needed to confirm and better understand these potential associations
246 and mechanisms. In contrast, the *TARDBP* (p.L248F) variant was validated only in the original
247 primary motor cortex sample at very low VAF (~0.5%) by both amplicon sequencing and
248 ddPCR, but was not detected in sorted cell fractions from an additional adjacent primary motor
249 cortex sample, indicating a highly focal event.
250
251 **RNA-MosaicHunter identifies additional predicted deleterious somatic variants in bulk**
252 **RNA-seq data of sALS cases**
253 To complement our targeted sequencing of neurodegenerative genes, which identified predicted
254 deleterious somatic variants in a small proportion of sALS and sFTD cases, we performed a
255 transcriptome-wide screen for somatic variants using bulk RNA-seq data to explore whether
256 previously unknown genes might cause disease in a mosaic state. We profiled predicted
257 deleterious somatic variants across all expressed genes in bulk RNA-seq data from 789
258 postmortem brain and spinal cord tissue samples of 143 sALS cases and 23 age-matched controls
259 generated by the New York Genome Center ALS Consortium (Supplementary Table 9; 81 sALS
260 and 11 control cases overlapped with our MIP cohort) using RNA-MosaicHunter[53], which
261 detects clonal somatic variants from bulk RNA-seq data using a Bayesian probabilistic model.
262 Due to limited bulk RNA-seq depth, this approach is sensitive only to somatic variants with
263 VAFs > ~5% and does not detect somatic variants at ultra-low levels.
264 Although we did not observe a significant increase in the burden of total or predicted
265 deleterious somatic variants in germline-free sALS cases (Supplementary Fig. 3), we identified
266 predicted deleterious somatic SNVs in *DYNC1H1* and *LMNA* in multiple CNS regions of two
267 sALS cases lacking other pathogenic or predicted deleterious germline/somatic variants (Fig. 5a
268 and Supplementary Table 10); both cases overlapped with our MIP cohort. Heterozygously
269 acting, generally *de novo*, variants in *DYNC1H1* and *LMNA* have been found in patients with
270 phenotypes resembling spinal muscular atrophy (SMA)[54-57], a motor neuron disease genetically
271 distinct but sharing some pathological overlap with ALS[58]. Both individuals presented with leg-
272 onset ALS and predominant spinal cord TDP-43 pathology (Fig. 5a-c). Amplicon sequencing
273 revealed broad CNS distribution of the *LMNA* (p.H566Y) variant (VAF 5.3-12.3%) and the
274 *DYNC1H1* (p.R1962C) variant (VAF 0.1-5.2%), with the *DYNC1H1* variant extremely low in
275 the cerebellum (0.1%), thoracic spinal cord (0.8%) and lumbar spinal cord (0.8%) (Fig. 5d and
276 Supplementary Table 8). Notably, the *DYNC1H1* (p.R1962C) variant was undetectable in
277 cultured fibroblasts from the patient (Supplementary Table 8), indicating a late developmental,

CNS-restricted origin. The broad CNS distribution of these variants aligns with our previous observations that somatic variants above ~5% VAFs are typically detected across the CNS[59], with lower regional VAFs potentially reflecting selective neuronal loss. The *DYNC1H1* p.R1962C variant is highly pathogenic, as it completely abolishes dynein motor function *in vitro*[60], and causes severe malformations of cortical development and delayed psychomotor development in patients carrying this germline variant[61,62]. Although the *LMNA* (p.H566Y) variant was not previously reported, germline *LMNA* variants cause autosomal dominant laminopathies with early lethality, including Hutchinson-Gilford progeria and congenital muscular dystrophy[63,64]. Thus, germline variants in both genes would ordinarily preclude ALS, but the mosaic state may allow for a normal early life followed by late-onset neurodegeneration. These findings suggest that further genome-wide exploration of brain tissue for somatic variants could reveal additional ALS genes that cause early lethality in the germline state.

Somatic *C9orf72* repeat expansions detected by targeted long-read sequencing

The germline *C9orf72* repeat expansion is the most common genetic cause of ALS and FTD[27,28]. Repeat lengths > 30 are generally considered pathogenic, with most affected individuals carrying hundreds to thousands of repeats. Intermediate expansions with 20-30 repeats, confer an increased disease risk, while expansions with < 20 repeats are regarded as normal[27,65]. While, instability of pathogenic repeat expansions (> 30 repeats) across tissues within the same individual has been reported[66-68], somatic expansion from non-expanded alleles has not been described. In our ALS and FTD cohort, the repeat-primed PCR analysis identified four ALS and FTD cases with both wild-type and expanded alleles showing reduced repeat peak heights[69] (Extended Data Fig. 9), suggestive of somatic expansion. Targeted long-read sequencing in brain tissues from these cases confirmed the presence of both wild-type and expanded alleles with dozens to thousands of repeats. Remarkably, one FTD case carried two short wild-type alleles (4 and 9 repeats), together with highly expanded pathogenic alleles (Fig. 6a). Haplotype phasing based on heterozygous single-nucleotide polymorphisms (SNPs) flanking the repeat expansions showed that all expanded alleles shared the same SNP haplotype as the 4-repeat allele (Fig. 6b), strongly suggesting spontaneous somatic *C9orf72* repeat expansion of a non-expanded allele, though future analysis of more cases is needed to further characterize this possibility. In the remaining three cases, one wild-type allele and a spectrum of expanded alleles were detected, with minimum repeat sizes of 20, 56, and 64 repeats (Extended Data Fig. 10), consistent with somatic expansion from intermediate or short pathogenic alleles, although the possibility of contraction cannot be excluded. Together, these findings suggest that somatic *C9orf72* repeat expansions may contribute to sporadic ALS and FTD. Nevertheless, even long-read sequencing lacked sufficient sensitivity to comprehensively assess all germline-free cases (see Discussion), and the prevalence of somatic *C9orf72* expansions remains to be determined.

Discussion

Our data provide several important insights into sALS and sFTD. First, approximately 30% of disease cases carried pathogenic or predicted deleterious germline variants in ALS/FTD genes, although our pathogenicity prediction might be overestimated. This advocates for a shift from family history-based to genetic testing-based disease classification, consistent with recently published guidelines for ALS genetic testing and counseling[70]. Second, a small but significant fraction (~2.1%) of germline-free sporadic cases harbored predicted deleterious somatic variants in known ALS or FTD genes, with disease- and region-specific distributions in ALS, providing

324 proof of concept for a contribution of somatic variants to disease pathogenesis. In addition, we
325 identified genes associated with severe pediatric degenerative diseases that may contribute to
326 ALS in the somatic state, broadening the spectrum of potential disease genes. Finally, targeted
327 long-read sequencing revealed somatic *C9orf72* repeat expansions arising from wild-type,
328 intermediate, and short pathogenic alleles in ALS and FTD cases.
329 While the case-control enrichment of somatic variants supports a pathogenic role, these
330 variants occurred at surprisingly low VAFs and showed topographic restriction consistent with
331 focal disease onset. Such variants likely arose late in development and were not shared by other
332 tissue regions, exemplified by the *TARDBP* (p. L248F) variant detectable only at its site of
333 discovery. The focal nature of these events would preclude detection by routine genetic testing
334 with blood or other peripheral samples and support a mechanism by which degeneration may
335 spread from a site containing mutant cells to anatomically connected regions, perhaps via
336 intercellular transmission of TDP-43 proteinopathy[12-18,71,72]. The identification of predicted
337 deleterious somatic variants in the primary motor cortex or spinal cord from individuals with
338 ALS suggests that ALS may initiate in UMNs or LMNs before involving both.
339 While performed on a limited number of variants, our cell-type analysis revealed that
340 several predicted deleterious somatic variants were shared across cell types and enriched in glia
341 compared to neurons. However, this apparent glial enrichment may reflect preferential loss of
342 neurons carrying these variants, consistent with their enrichment in hypodiploid cells, a
343 population likely associated with apoptotic cell death. Together, these findings support a model
344 in which deleterious somatic variants contribute to focal disease initiation, with subsequent
345 neuronal loss leading to reduced VAFs over time.
346 Although only ~2.1% of germline-free disease cases carried predicted deleterious somatic
347 variants in ALS/FTD genes in our MIP sequencing data, this is likely greatly underestimated due
348 to limited sensitivity for detecting ultra-low-VAF variants (Extended Data Fig. 1). Detecting
349 such variants remains technically challenging[46], and broader sampling across CNS regions is also
350 limited. However, future duplex sequencing approaches promise the ability to define the minimal
351 VAFs capable of initiating disease. On the other hand, several of our statistical comparisons
352 approached nominal significance, highlighting the need for larger cohorts and more sensitive
353 approaches.
354 While MIP sequencing did not allow for detection of somatic *C9orf72* repeat expansions
355 in our samples, targeted long-read sequencing identified ALS and FTD cases with somatic
356 expansions of varying repeat sizes, including an FTD case carrying two wild-type and highly
357 expanded alleles, consistent with *de novo* expansion. These findings suggest that somatic
358 *C9orf72* repeat expansions may contribute to sporadic ALS and FTD and could exhibit cell-type-
359 specific patterns of expansion, analogous to somatic *HTT* CAG repeat expansion in striatal
360 projection neurons[73]. However, the current targeted long-read sequencing approach preferentially
361 enriches shorter alleles and provides limited flanking sequence, precluding accurate VAF
362 estimation and robust haplotype phasing. Future targeted long-read sequencing with extended
363 flanking coverage will be required to determine the origin and prevalence of somatic *C9orf72*
364 repeat expansions.
365 Finally, the identification of somatic SNVs in *DYNC1H1* and *LMNA* suggests that genes
366 predisposing to ALS and FTD in the somatic state may extend beyond those identified in
367 germline studies. Although certain alleles in these genes cause motor neuron degeneration in the
368 form of SMA, other alleles—including *DYNC1H1* p. R1962C[61,62]—cause severe pediatric
369 disease that would preclude late-life ALS in the germline but may be compatible with disease in

370 the somatic state. Similarly, enrichment in germline-free FTD cases emerged only when all
371 targeted neurodegenerative genes were considered, hinting at a wider array of FTD-related
372 genes. Together, these findings highlight the potential of future genome-wide approaches to
373 uncover additional somatic genetic mechanisms and illuminate the topographic spread of
374 pathology from focal origins.
375

Acknowledgements

We thank the Massachusetts Alzheimer's Disease Research Center, Oxford Brain Bank, Target ALS Foundation (Biobank Core Facility at St. Joseph's Hospital and Barrow Neurological Institute, Georgetown Brain Bank, Eleanor and Lou Gehrig ALS Center at Columbia University and UCSD ALS bank) and NIH NeuroBioBank (Harvard Brain Tissue Resource Center, Mount Sinai/JJ Peters VA Medical Center NIH Brain and Tissue Repository, Brain Endowment Bank of University of Miami, University of Pittsburgh Neuropathology Brain Bank, University of Maryland Brian and Tissue Bank and UCLA Human Brain and Spinal Fluid Resource Center) for providing fresh frozen human tissues. We thank the Target ALS Human Postmortem Tissue Core, New York Genome Center for Genomics of Neurodegenerative Disease, Amyotrophic Lateral Sclerosis Association and TOW Foundation for providing the bulk RNA-seq data. We thank the donors and families for their contributions, and J. E. Neil and J. Gonzalez for assistance with tissue procurement. We thank the Research Computing group at Harvard Medical School and Boston Children's Hospital. The brains in Figures 4 and 5 were illustrated by A. Lai with input from the authors. This work was supported by the PRMRP Discovery Award W81XWH2010028 (Z.Z.); the Edward R. and Anne G. Lefler Center postdoctoral fellowship (Z.Z.); the American Heart Association Career Development Award 23CDA1046074 (Z.Z.); the National Research Foundation of Korea (NRF) 2022R1C1C1010430 (Junho K.); RS-2023-00217881 (Junho K.); RS-2025-02215360 (Junho K.); R01 AG088082 (A.Y.H.); the Alzheimer's Association research fellowship (A.Y.H.); R56 AG079857 (A.Y.H., C.A.W. and E.A.L.); a Cullen Education and Research Foundation Young Investigator Award from the Healey Center (M.N.); a Holloway Postdoctoral Fellowship from the Association for Frontotemporal Degeneration (M.N.); K08 AG065502 (M.B.M.); donors of the Alzheimer's Disease Research program of the BrightFocus Foundation A20201292F (M.B.M.); the Doris Duke Charitable Foundation Clinical Scientist Development Award 2021183 (M.B.M.); K01 AG051791 (E.A.L.); the Suh Kyungbae Foundation (E.A.L.), DP2 AG072437 (E.A.L.); R01 NS032457 (C.A.W.); R01 AG070921 (C.A.W. and E.A.L.); a Massachusetts Alzheimer's Disease Research Center pilot grant (C.L.-T. and C.A.W.); and the Allen Discovery Center program, a Paul G. Allen Frontiers Group advised program of the Paul G. Allen Family Foundation (C.A.W. and E.A.L.). C.L.-T. is supported by the Araminta Broch-Healey Endowed Chair in ALS. C.A.W. is an Investigator of the Howard Hughes Medical Institute. The funders had no role in the study design, data collection and analysis, decision to publish or preparation of the manuscript.

Author Contributions

Z.Z., Junho K., A.Y.H., E.A.L., C.L.-T. and C.A.W. conceived and designed the study. Z.Z. performed tissue processing, MIP panel sequencing, cell sorting, amplicon sequencing, and targeted long-read sequencing. Junho K. performed bioinformatic analysis for MIP and validation data with assistance from R.D., T.S., and B.Z. A.Y.H. performed bioinformatic analysis for bulk RNA-seq data with assistance from J.P. and M.B. Jinhyeong K. performed bioinformatic analysis for long-read sequencing data. M.N. optimized and performed immunofluorescent imaging and quantification, and generated data shown in this manuscript. Z.Z., M.B.M. and R.D. designed the MIP panel. B.C., K.M., R.C.Y., and C.-Z.L. helped with tissue processing and amplicon sequencing. C.K. provided technical support for MIP sequencing. J.E.N. contributed tissue procurement and ethics expertise. T.O. and J.R. provided immunofluorescent images and interpretation of disease pathology. L.W.O. and O.A. provided

fresh frozen human tissues and interpretation of disease pathology. C.L.-T., E.A.L. and C.A.W. supervised the study. Z.Z., Junho K., A.Y.H., C.L.-T., E.A.L. and C.A.W., wrote the manuscript.

Competing Interests

C.L.-T serves on the scientific advisory board and/or has received consulting fees from SOLA Biosciences, Libra Therapeutics, Arbor Biotechnologies, Dewpoint Therapeutics, Mitsubishi Tanabe Pharma Holdings America, Sanofi, AUTTX LLC, Carthera, the Milken Institute, and Applied Genetic Technologies Corporation. E.A.L. serves on the scientific advisory board of Genome Insight. C.A.W. is a paid consultant (cash, no equity) to CAMP4 Therapeutics (cash, no equity), Maze Therapeutics (cash and equity), is a member of the scientific advisory board for Bioskryb Genomics, Inc., (cash) and is a founding advisor for Mosaica Medicines (equity). These companies did not fund and had no role in the conception or performance of this research project.

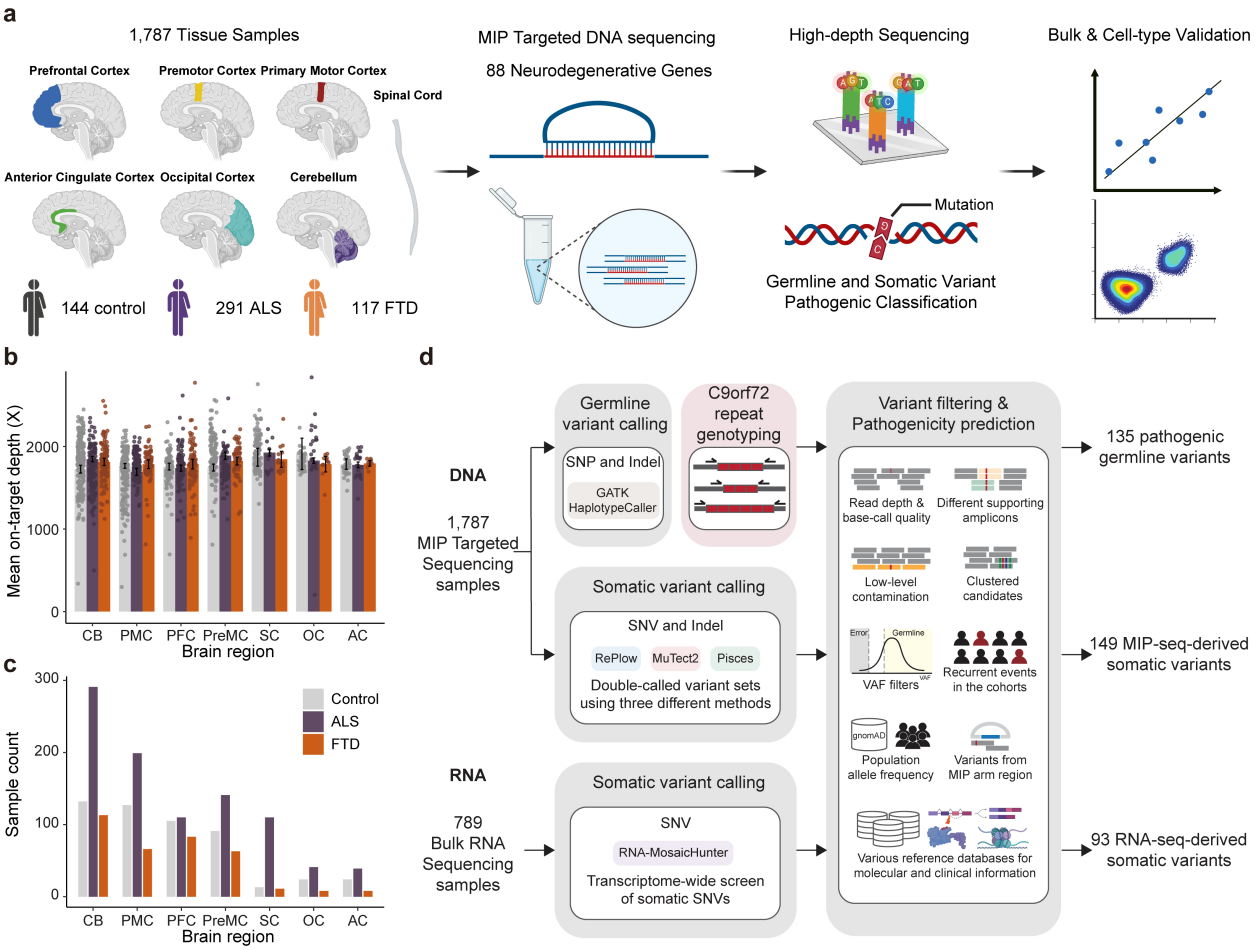

Fig. 1 | Experimental and analysis strategies. **a**, Overall scheme of the experiments. Genomic DNA isolated from 1,787 postmortem tissue samples of multiple brain regions and spinal cords of 144 control, 291 ALS, and 117 FTD cases were used for molecular inversion probe (MIP) capture sequencing with ultra-high depth. Created with BioRender.com. **b**,**c**, Mean sequencing depth (**b**) and number of tissue samples (**c**) in different brain regions and spinal cords of control, ALS, and FTD cases. Control, $n = 516$; ALS, $n = 938$; FTD, $n = 375$. Note that 42 samples from 9 ALS-FTD cases were included in both conditions. CB, cerebellum; PMC, primary motor cortex; PFC, prefrontal cortex; PreMC, premotor cortex; SC, spinal cord; OC, occipital cortex; AC, anterior cingulate cortex. Error bars, 95% CI. **d**, Methodological pipelines to identify germline and somatic variants. Germline variants were called by GATK HaplotypeCaller. *C9orf72* genotype of ALS and FTD cases were determined by repeat-primed PCR. Somatic variants were called by RePlow, MuTect2, and Pisces. Additional somatic variants were called from 789 bulk RNA-seq profiles of multiple brain regions and spinal cords of ALS cases generated by the New York Genome Center ALS Consortium using RNA-MosaicHunter. Created with BioRender.com.

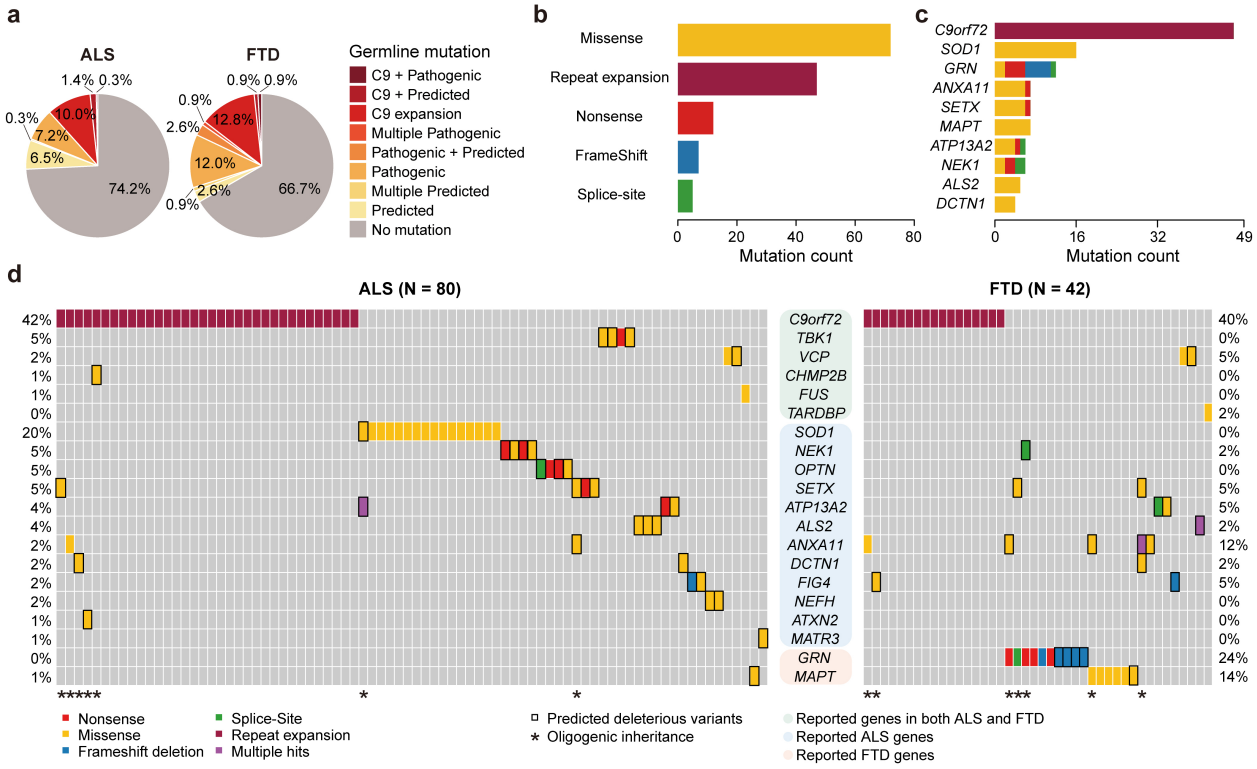

Fig. 2 | *C9orf72* repeat expansion and pathogenic germline variants in ALS/FTD genes are prevalent in ALS and FTD. a, Proportions of ALS and FTD cases with *C9orf72* repeat expansion, pathogenic, and predicted deleterious germline variants in ALS/FTD genes. Cases with multiple predicted deleterious variants are indicated with '+' sign. Note that cases with a heterozygous variant in recessive genes (e.g., *ALS2*, *ATP13A2*) are not included in the proportions. **b**, Distribution of *C9orf72* repeat expansion, pathogenic, and predicted deleterious germline variants in ALS/FTD genes classified by variant types. **c**, Ranking of the top 10 mutated ALS/FTD genes. **d**, Visualization of ALS and FTD cases (vertical columns) with pathogenic and predicted deleterious germline variants (horizontal rows) in ALS/FTD genes. Color codes indicate the types of variants. Rectangular outline represents predicted deleterious variants. Genes are grouped by their known involvement in the diseases. * indicates cases with multiple pathogenic or predicted deleterious variants.

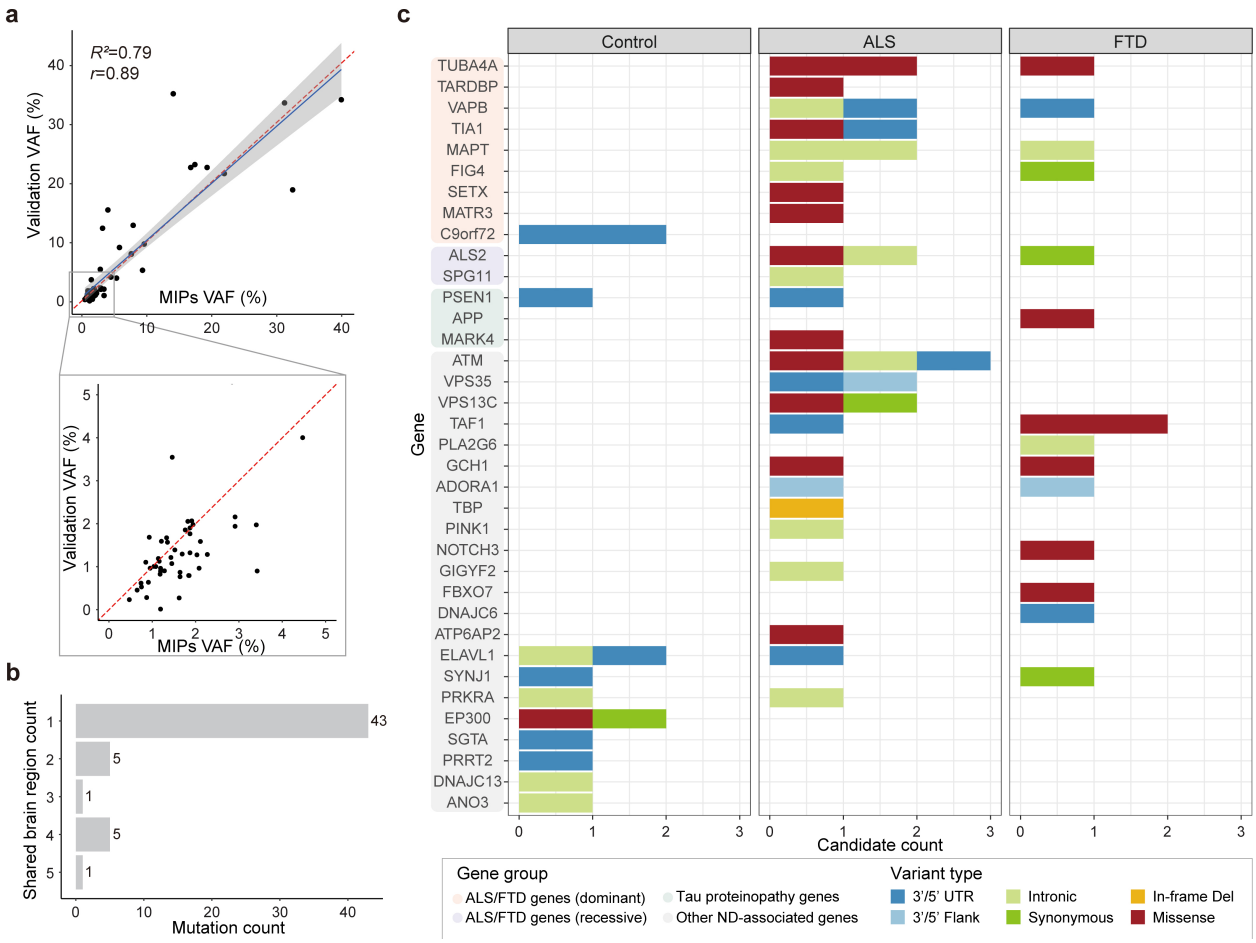

Fig. 3 | Somatic variants in MIP sequencing data tend to be focal, protein-altering, and are almost exclusively restricted to disease cases. a, The observed VAFs of somatic variants in amplicon sequencing validation were consistent with the VAFs in original MIP sequencing. Sixty-four somatic variants were validated and included in the plot. Shaded band, 95% CI of the fitted linear regression. **b**, Total somatic variant counts classified by the number of brain regions in which a given variant was identified. **c**, Distribution of somatic variants in all neurodegenerative genes. Genes are categorized into four groups: ALS/FTD-related dominant genes, ALS/FTD-related recessive genes, Tau proteinopathy-related genes, and other neurodegeneration/dementia-associated genes. Color codes indicate variant types. Note that somatic variants identified in controls are unlikely to alter function, with just one missense variant (red) and the remaining being synonymous or noncoding substitutions.

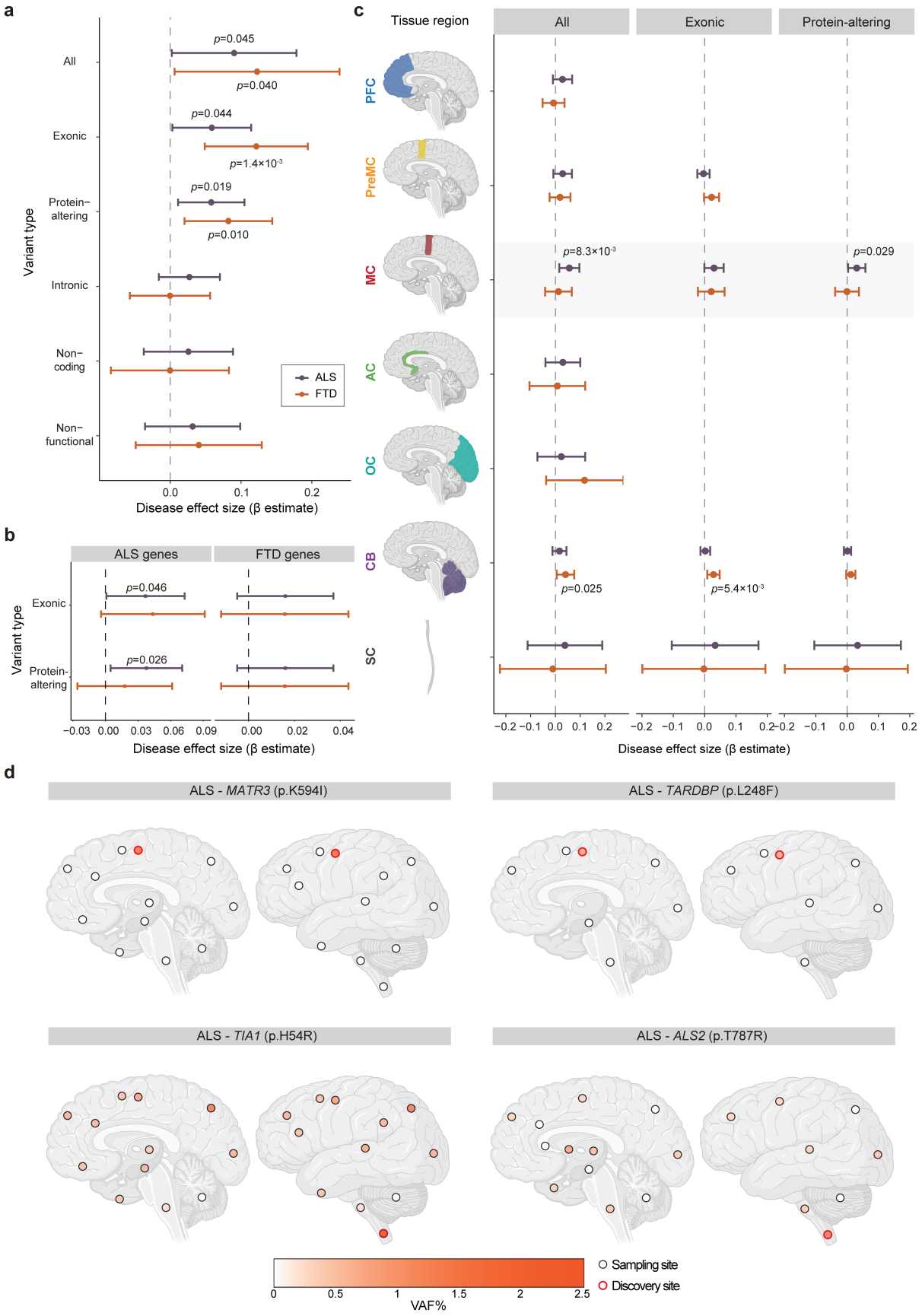
a
All
Exonic
Protein−altering
Intronic
Non−coding
Non−functional
Variant type
p=0.045
p=0.040
p=0.044
p=1.4×10-3
p=0.019
p=0.010
ALS
FTD
0.0
0.1
0.2
Disease effect size (β estimate)
b
ALS genes
FTD genes
Exonic
Protein-altering
Variant type
p=0.046
p=0.026
−0.03 0.00 0.03 0.06 0.09
0.00 0.02 0.04
Disease effect size (β estimate)
c
Tissue region
PFC
PreMC
MC
AC
OC
CB
SC
All
Exonic
Protein-altering
p=8.3×10-3
p=0.029
p=0.025
p=5.4×10-3
−0.2 −0.1 0.0 0.1 0.2
Disease effect size (β estimate)
d
ALS - MATR3 (p.K594I)
ALS - TARDBP (p.L248F)
ALS - TIA1 (p.H54R)
ALS - ALS2 (p.T787R)
0 0.5 1 1.5 2 2.5
VAF%
Sampling site
Discovery site

483

484 **Fig. 4 | Somatic variants are enriched in ALS and FTD cases and disease-related tissue**
485 **regions**. **a**, Enrichment of somatic variants in different genomic regions of germline-free ALS
486 and FTD cases compared to normal controls. **b**, Enrichment of exonic and protein-altering
487 somatic variants in two different groups of disease-related genes (ALS genes and FTD genes)
488 compared to normal controls. **c**, Enrichment of somatic variants in ALS/FTD genes across
489 different brain regions of germline-free ALS and FTD cases compared to normal controls.
490 Missing points indicate no variants were observed. **a-c**, Disease effect sizes were estimated using
491 an individual-wise linear mixed-effects model by comparing variant burden per germline-free
492 disease individual with that of normal individuals (see Methods). Significance and 95% CI were
493 estimated while controlling for potential confounding factors, including average read depth, sex,
494 post-mortem interval, sequencing batch, and number of samples per donor. Sample sizes were:
495 control, $n = 144$; ALS, $n = 216$; FTD, $n = 78$ (biological replicates). Unadjusted P values are
496 shown, as the tests examine biologically distinct but non-independent categories with differing
497 background mutation structures. Created with BioRender.com. **d**, Regional distribution of VAFs
498 of several predicted deleterious somatic variants in individual brains and spinal cords. Brain
499 cortex is annotated by Brodmann areas. The color spectrum indicates the VAFs of somatic
500 variants in amplicon sequencing. White indicates regions without the somatic variants. Red
501 highlight indicates the region of initial detection by MIP sequencing. Created with
502 BioRender.com.
503

a

Individual	Gender	Disease	Onset	Age	Variant	Tissue	VAF
NEUEL133AK6	Female	ALS	Leg	61	*DYNC1H1* (p.R1962C)	Frontal cortex	0.054
						Medial motor cortex	0.036
						Lateral motor cortex	0.042
						Cervical SC	0.021
						Thoracic SC	0.022
						Lumbar SC	0.036
NEUMY028JH4	Female	ALS	Leg	54	*LMNA* (p.H566Y)	Frontal cortex	0.125
						Medial motor cortex	0.179
						Cervical SC	0.172
						Thoracic SC	0.169
						Lumbar SC	0.075

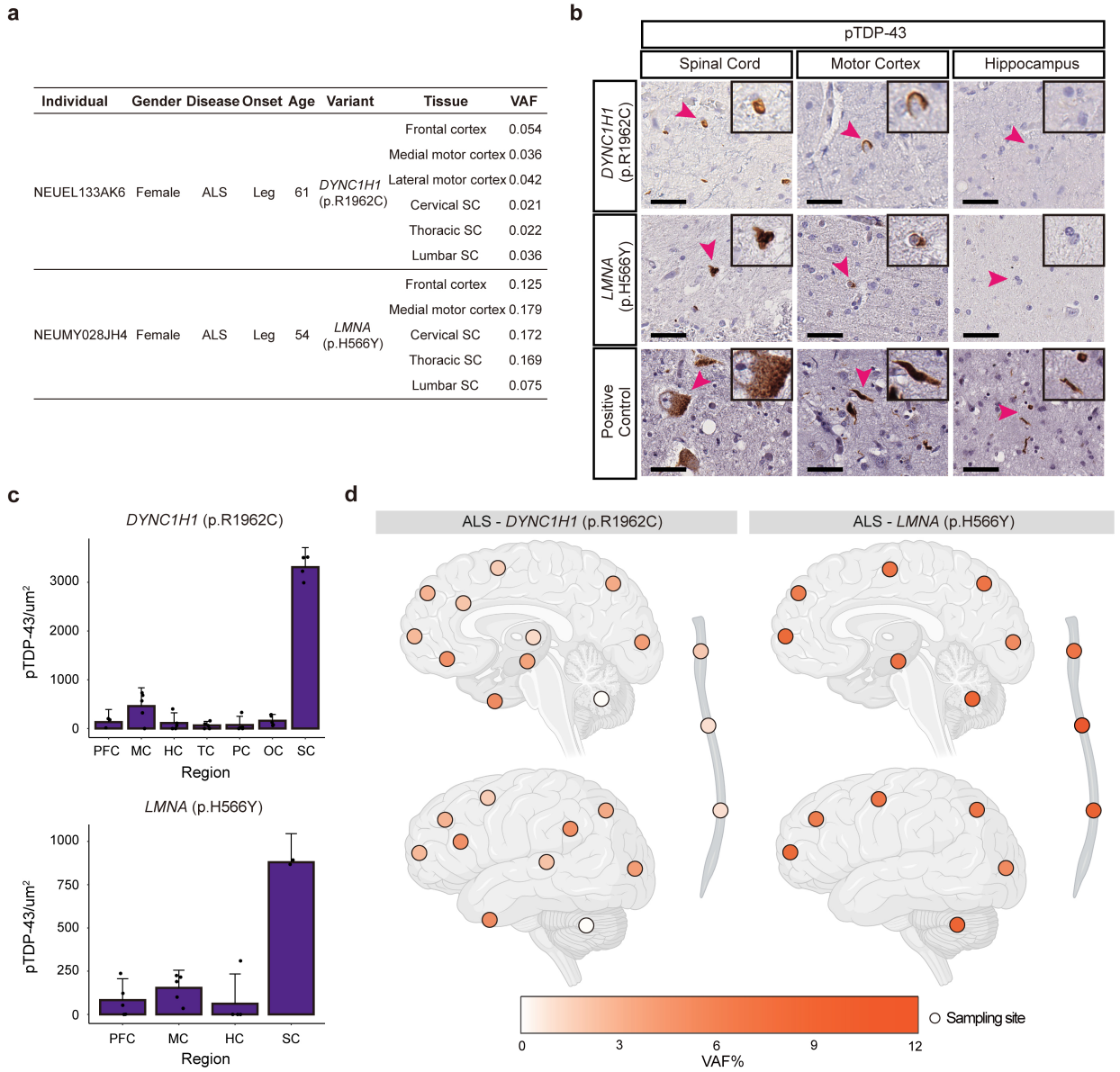

Fig. 5 | Somatic variants in *DYNC1H1* and *LMNA* in sALS. a, Two deleterious somatic SNVs that were shared by multiple tissue regions of the ALS cases. **b**, Sections of the lumbar spinal cord, motor cortex, and hippocampus of the two sALS cases stained with a phospho-TDP43 antibody. Scale bar, 40 µm. Arrowheads indicate the cells shown in the insets, which are magnified to twice their original size. **c**, Quantification of phospho-TDP43 staining of CNS tissue sections of the two sALS cases with *DYNC1H1* and *LMNA* somatic variants. For *DYNC1H1*, tissue-section-level biological replicates included 3 from PFC, 4 from SC, and 5 from MC, HC, TC, PC, and OC. For *LMNA*, tissue-section-level biological replicates included 2 from SC and 5 from PFC, MC, and HC. Bar graph, mean ± 95% CI. PFC, prefrontal cortex; MC, primary motor cortex; HC, hippocampus; TC, temporal cortex; PC, parietal cortex; OC, occipital cortex; SC, spinal cord. **d**, Regional distribution of VAFs of somatic variants in individual brains and spinal cords. Brain cortex is annotated by Brodmann areas. The color spectrum indicates the

518 VAFs of somatic variants in amplicon sequencing. White indicates regions without the somatic
519 variants. Created with BioRender.com.
520

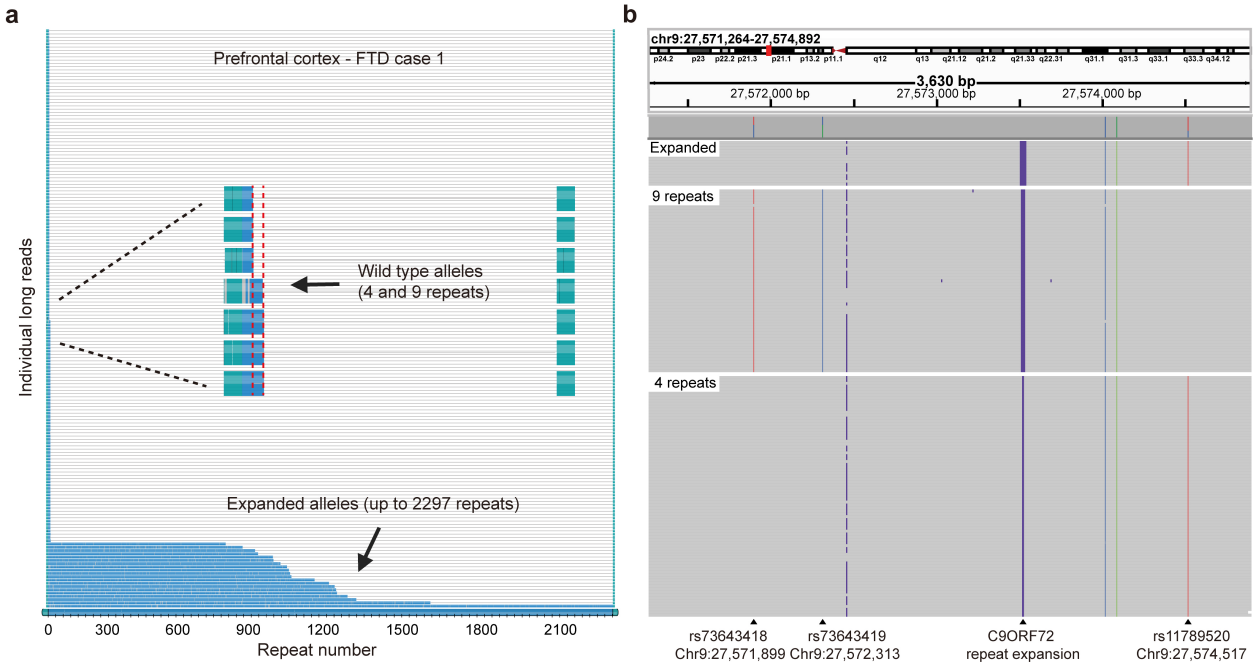

Fig. 6 | Somatic *C9orf72* repeat expansion in an FTD case. a, Waterfall plot showing targeted long-read sequencing results from the prefrontal cortex tissue of a sporadic FTD case. Two wild-type alleles with 4 and 9 repeats, respectively, are observed, along with somatic *C9orf72* repeat expansions ranging from 748 to 2,297 repeats. Each row represents an individual long read; the *C9orf72* repeat region is shown in blue, and the flanking regions are shown in green. Red dashed lines mark the sizes of the wild-type alleles. The *x*-axis denotes the number of GGGGCC hexanucleotide repeats. **b**, IGV screenshot showing haplotype phasing based on SNPs flanking the *C9orf72* repeat expansion. Long reads are grouped by repeat size category (expanded, 9 repeats, 4 repeats). SNPs rs73643418, rs73643419, and rs11789520 are heterozygous in this individual. All expanded alleles share the same SNP haplotype as the 4-repeat allele.

534 **References**

535 1. Ferrari, R., Kapogiannis, D., Huey, E. D. & Momeni, P. FTD and ALS: a tale of two
536 diseases. *Curr. Alzheimer Res.* **8**, 273-294 (2011).
537 2. Saxon, J. A. *et al.* Examining the language and behavioural profile in FTD and ALS-
538 FTD. *J. Neurol. Neurosurg. Psychiatry* **88**, 675-680 (2017).
539 3. Lagier-Tourenne, C., Polymenidou, M. & Cleveland, D. W. TDP-43 and FUS/TLS:
540 emerging roles in RNA processing and neurodegeneration. *Hum. Mol. Genet.* **19**, R46-
541 R64 (2010).
542 4. Ling, S. C., Polymenidou, M. & Cleveland, D. W. Converging mechanisms in ALS and
543 FTD: disrupted RNA and protein homeostasis. *Neuron* **79**, 416-438 (2013).
544 5. Ravits, J. M. & La Spada, A. R. ALS motor phenotype heterogeneity, focality, and
545 spread: deconstructing motor neuron degeneration. *Neurology* **73**, 805-811 (2009).
546 6. Kanouchi, T., Ohkubo, T. & Yokota, T. Can regional spreading of amyotrophic lateral
547 sclerosis motor symptoms be explained by prion-like propagation? *J. Neurol. Neurosurg.*
548 *Psychiatry* **83**, 739-745 (2012).
549 7. Eisen, A., Kim, S. & Pant, B. Amyotrophic lateral sclerosis (ALS): a phylogenetic
550 disease of the corticomotoneuron? *Muscle Nerve* **15**, 219-224 (1992).
551 8. Chou, S. M. & Norris, F. H. Amyotrophic lateral sclerosis: lower motor neuron disease
552 spreading to upper motor neurons. *Muscle Nerve* **16**, 864-869 (1993).
553 9. Gromicho, M. *et al.* Spreading in ALS: the relative impact of upper and lower motor
554 neuron involvement. *Ann. Clin. Transl. Neurol.* **7**, 1181-1192 (2020).
555 10. Brettschneider, J. *et al.* Stages of pTDP-43 pathology in amyotrophic lateral sclerosis.
556 *Ann. Neurol.* **74**, 20-38 (2013).
557 11. Brettschneider, J. *et al.* Sequential distribution of pTDP-43 pathology in behavioral
558 variant frontotemporal dementia (bvFTD). *Acta Neuropathol.* **127**, 423-439 (2014).
559 12. Polymenidou, M. & Cleveland, D. W. Biological spectrum of amyotrophic lateral
560 sclerosis prions. *Cold Spring Harb. Perspect. Med.* **7**, a024133 (2017).
561 13. Porta, S. *et al.* Patient-derived frontotemporal lobar degeneration brain extracts induce
562 formation and spreading of TDP-43 pathology in vivo. *Nat. Commun.* **9**, 4220 (2018).
563 14. Laferriere, F. *et al.* TDP-43 extracted from frontotemporal lobar degeneration subject
564 brains displays distinct aggregate assemblies and neurotoxic effects reflecting disease
565 progression rates. *Nat. Neurosci.* **22**, 65-77 (2019).
566 15. Peng, C., Trojanowski, J. Q. & Lee, V. M. Protein transmission in neurodegenerative
567 disease. *Nat. Rev. Neurol.* **16**, 199-212 (2020).
568 16. De Rossi, P. *et al.* FTLD-TDP assemblies seed neoaggregates with subtype-specific
569 features via a prion-like cascade. *EMBO Rep.* **22**, e53877 (2021).
570 17. Tamaki, Y. *et al.* Spinal cord extracts of amyotrophic lateral sclerosis spread TDP-43
571 pathology in cerebral organoids. *PLoS Genet.* **19**, e1010606 (2023).
572 18. Kumar, S. T. *et al.* Seeding the aggregation of TDP-43 requires post-fibrillization
573 proteolytic cleavage. *Nat. Neurosci.* **26**, 983-996 (2023).
574 19. Rosen, D. R. *et al.* Mutations in Cu/Zn superoxide dismutase gene are associated with
575 familial amyotrophic lateral sclerosis. *Nature* **362**, 59-62 (1993).
576 20. Turner, M. R. *et al.* Controversies and priorities in amyotrophic lateral sclerosis. *Lancet*
577 *Neurol.* **12**, 310-322 (2013).

578 21. Wang, H. *et al.* Smoking and risk of amyotrophic lateral sclerosis: a pooled analysis of 5
579 prospective cohorts. *Arch. Neurol.* **68**, 207-213 (2011).
580 22. Armon, C. Acquired nucleic acid changes may trigger sporadic amyotrophic lateral
581 sclerosis. *Muscle Nerve* **32**, 373-377 (2005).
582 23. Jamuar, S. S. *et al.* Somatic mutations in cerebral cortical malformations. *N. Engl. J.*
583 *Med.* **371**, 733-743 (2014).
584 24. Proukakis, C. Somatic mutations in neurodegeneration: an update. *Neurobiol. Dis.* **144**,
585 105021 (2020).
586 25. Hardenbol, P. *et al.* Multiplexed genotyping with sequence-tagged molecular inversion
587 probes. *Nat. Biotechnol.* **21**, 673-678 (2003).
588 26. Wang, K., Li, M. & Hakonarson, H. ANNOVAR: functional annotation of genetic
589 variants from high-throughput sequencing data. *Nucleic Acids Res.* **38**, e164 (2010).
590 27. Renton, A. E. *et al.* A hexanucleotide repeat expansion in *C9ORF72* is the cause of
591 chromosome 9p21-linked ALS-FTD. *Neuron* **72**, 257-268 (2011).
592 28. DeJesus-Hernandez, M. *et al.* Expanded GGGGCC hexanucleotide repeat in noncoding
593 region of *C9ORF72* causes chromosome 9p-linked FTD and ALS. *Neuron* **72**, 245-256
594 (2011).
595 29. Majounie, E. *et al.* Frequency of the C9orf72 hexanucleotide repeat expansion in patients
596 with amyotrophic lateral sclerosis and frontotemporal dementia: a cross-sectional study.
597 *Lancet Neurol.* **11**, 323-330 (2012).
598 30. Byrne, S. *et al.* Cognitive and clinical characteristics of patients with amyotrophic lateral
599 sclerosis carrying a C9orf72 repeat expansion: a population-based cohort study. *Lancet*
600 *Neurol.* **11**, 232-240 (2012).
601 31. Mahoney, C. J. *et al.* Frontotemporal dementia with the C9ORF72 hexanucleotide repeat
602 expansion: clinical, neuroanatomical and neuropathological features. *Brain* **135**, 736-750
603 (2012).
604 32. Baker, M. *et al.* Mutations in progranulin cause tau-negative frontotemporal dementia
605 linked to chromosome 17. *Nature* **442**, 916-919 (2006).
606 33. Cruts, M. *et al.* Null mutations in progranulin cause ubiquitin-positive frontotemporal
607 dementia linked to chromosome 17q21. *Nature* **442**, 920-924 (2006).
608 34. van Blitterswijk, M. *et al.* Evidence for an oligogenic basis of amyotrophic lateral
609 sclerosis. *Hum. Mol. Genet.* **21**, 3776-3784 (2012).
610 35. Testi, S., Tamburin, S., Zanette, G. & Fabrizi, G. M. Co-occurrence of the *C9ORF72*
611 expansion and a novel GRN mutation in a family with alternative expression of
612 frontotemporal dementia and amyotrophic lateral sclerosis. *J. Alzheimers Dis.* **44**, 49-56
613 (2015).
614 36. Kuuluvainen, L. *et al.* Oligogenic basis of sporadic ALS: the example of SOD1
615 p.Ala90Val mutation. *Neurol. Genet.* **5**, e335 (2019).
616 37. Goutman, S. A. *et al.* Emerging insights into the complex genetics and pathophysiology
617 of amyotrophic lateral sclerosis. *Lancet Neurol.* **21**, 465-479 (2022).
618 38. Kim, J. *et al.* The use of technical replication for detection of low-level somatic
619 mutations in next-generation sequencing. *Nat. Commun.* **10**, 1047 (2019).
620 39. Benjamin, D. *et al.* Calling somatic SNVs and indels with Mutect2. *bioRxiv*, 861054
621 (2019).
622 40. Dunn, T. *et al.* Pisces: an accurate and versatile variant caller for somatic and germline
623 next-generation sequencing data. *Bioinformatics* **35**, 1579-1581 (2019).

624 41. Barnell, E. K. *et al.* Open-sourced CIViC annotation pipeline to identify and annotate
625 clinically relevant variants using single-molecule molecular inversion probes. *JCO Clin*
626 *Cancer Inform* **3**, 1-12 (2019).
627 42. Biezuner, T. *et al.* An improved molecular inversion probe based targeted sequencing
628 approach for low variant allele frequency. *NAR Genom. Bioinform.* **4**, lqab125 (2022).
629 43. Bizzotto, S. *et al.* Landmarks of human embryonic development inscribed in somatic
630 mutations. *Science* **371**, 1249-1253 (2021).
631 44. Lee, J. *et al.* Mutalisk: a web-based somatic MUTation AnaLyIS toolKit for genomic,
632 transcriptional and epigenomic signatures. *Nucleic Acids Res.* **46**, W102-W108 (2018).
633 45. Chung, C. *et al.* Comprehensive multi-omic profiling of somatic mutations in
634 malformations of cortical development. *Nat. Genet.* **55**, 209-220 (2023).
635 46. Huang, A. Y. & Lee, E. A. Identification of somatic mutations from bulk and single-cell
636 sequencing data. *Front. Aging* **2**, 800380 (2021).
637 47. Hadano, S. *et al.* A gene encoding a putative GTPase regulator is mutated in familial
638 amyotrophic lateral sclerosis 2. *Nat. Genet.* **29**, 166-173 (2001).
639 48. Yang, Y. *et al.* The gene encoding alsin, a protein with three guanine-nucleotide
640 exchange factor domains, is mutated in a form of recessive amyotrophic lateral sclerosis.
641 *Nat. Genet.* **29**, 160-165 (2001).
642 49. Darzynkiewicz, Z. *et al.* Features of apoptotic cells measured by flow cytometry.
643 *Cytometry* **13**, 795-808 (1992).
644 50. Arends, M. J., Morris, R. G. & Wyllie, A. H. Apoptosis. The role of the endonuclease.
645 *Am. J. Pathol.* **136**, 593-608 (1990).
646 51. Telford, W. G., King, L. E. & Fraker, P. J. Comparative evaluation of several DNA
647 binding dyes in the detection of apoptosis-associated chromatin degradation by flow
648 cytometry. *Cytometry* **13**, 137-143 (1992).
649 52. Del Bino, G., Lassota, P. & Darzynkiewicz, Z. The S-phase cytotoxicity of camptothecin.
650 *Exp. Cell Res.* **193**, 27-35 (1991).
651 53. Huang, A. Y. *et al.* Accurate detection of somatic single-nucleotide variants from bulk
652 RNA-seq data using RNA-MosaicHunter. *Nucleic Acids Res.* **54**, gkaf1450 (2026).
653 54. Rudnik-Schoneborn, S. *et al.* Mutations of the LMNA gene can mimic autosomal
654 dominant proximal spinal muscular atrophy. *Neurogenetics* **8**, 137-142 (2007).
655 55. Harms, M.B. *et al.* Mutations in the tail domain of *DYNC1H1* cause dominant spinal
656 muscular atrophy. *Neurology* **78**, 1714-1720 (2012).
657 56. Tsurusaki, Y. *et al.* A *DYNC1H1* mutation causes a dominant spinal muscular atrophy
658 with lower extremity predominance. *Neurogenetics* **13**, 327-332 (2012).
659 57. Iwahara, N., Hisahara, S., Hayashi, T., Kawamata, J. & Shimohama, S. A novel lamin
660 A/C gene mutation causing spinal muscular atrophy phenotype with cardiac involvement:
661 report of one case. *BMC Neurol.* **15**, 13 (2015).
662 58. Bowerman, M. *et al.* Pathogenic commonalities between spinal muscular atrophy and
663 amyotrophic lateral sclerosis: Converging roads to therapeutic development. *Eur. J. Med.*
664 *Genet.* **61**, 685-698 (2018).
665 59. Lodato, M. A. *et al.* Somatic mutation in single human neurons tracks developmental and
666 transcriptional history. *Science* **350**, 94-98 (2015).
667 60. Hoang, H. T., Schlager, M. A., Carter, A. P. & Bullock, S. L. *DYNC1H1* mutations
668 associated with neurological diseases compromise processivity of dynein-dynactin-cargo
669 adaptor complexes. *Proc. Natl. Acad. Sci. USA* **114**, E1597-E1606 (2017).

61. Poirier, K. *et al.* Mutations in *TUBG1*, *DYNC1H1*, *KIF5C* and *KIF2A* cause malformations of cortical development and microcephaly. *Nat. Genet.* **45**, 639-647 (2013).
62. Yang, H. *et al.* De novo variants in the *DYNC1H1* gene associated with infantile spasms. *Front. Neurol.* **12**, 733178 (2021).
63. Eriksson, M. *et al.* Recurrent de novo point mutations in lamin A cause Hutchinson-Gilford progeria syndrome. *Nature* **423**, 293-298 (2003).
64. Quijano-Roy, S. *et al.* De novo *LMNA* mutations cause a new form of congenital muscular dystrophy. *Ann. Neurol.* **64**, 177-186 (2008).
65. Breevoort, S., Gibson, S., Figueroa, K., Bromberg, M. & Pulst, S. Expanding clinical spectrum of *C9ORF72*-related disorders and promising therapeutic strategies: a Review. *Neurol. Genet.* **8**, e670 (2022).
66. van Blitterswijk, M. *et al.* Association between repeat sizes and clinical and pathological characteristics in carriers of *C9ORF72* repeat expansions (Xpansize-72): a cross-sectional cohort study. *Lancet Neurol.* **12**, 978-988 (2013).
67. DeJesus-Hernandez, M. *et al.* Long-read targeted sequencing uncovers clinicopathological associations for *C9orf72*-linked diseases. *Brain* **144**, 1082-1088 (2021).
68. Udine, E. *et al.* Targeted long-read sequencing to quantify methylation of the *C9orf72* repeat expansion. *Mol. Neurodegener.* **19**, 99 (2024).
69. Ross, J. P. *et al.* Somatic expansion of the *C9orf72* hexanucleotide repeat does not occur in ALS spinal cord tissues. *Neurol. Genet.* **5**, e317 (2019).
70. Roggenbuck, J. *et al.* Evidence-based consensus guidelines for ALS genetic testing and counseling. *Ann. Clin. Transl. Neurol.* **10**, 2074-2091 (2023).
71. Frank, S.A. Evolution in health and medicine Sackler colloquium: Somatic evolutionary genomics: mutations during development cause highly variable genetic mosaicism with risk of cancer and neurodegeneration. *Proc. Natl. Acad. Sci. USA* **107 Suppl 1**, 1725-1730 (2010).
72. Pamphlett, R. The "somatic-spread" hypothesis for sporadic neurodegenerative diseases. *Med. Hypotheses* **77**, 544-547 (2011).
73. Handsaker, R. E. *et al.* Long somatic DNA-repeat expansion drives neurodegeneration in Huntington's disease. *Cell* **188**, 623-639.e19 (2025).

704 **Methods**

705 **Tissue sources and sample preparation**

706 Fresh frozen postmortem human brain and spinal cord tissues were collected by the
707 Massachusetts Alzheimer's Disease Research Center, Oxford Brain Bank, Target ALS
708 Foundation, and NIH NeuroBioBank (Supplementary Table 1) according to their respective
709 institutional protocols, written authorization and informed consent; they were subsequently
710 obtained for this study with the approval of the Boston Children's Hospital Institutional Review
711 Board. Research on these deidentified specimens and data was performed at Boston Children's
712 Hospital with approval from the Committee on Clinical Investigation. Sporadic ALS and FTD
713 cases were selected based on available clinical records. ALS and FTD cases without clear
714 recording of family histories were also selected if the age of death was above 45 years old.
715 gDNA of these tissue samples was extracted using the EZ1 Advanced XL (Qiagen)
716 system followed by an additional purification using AMPure XP beads (Beckman Coulter).
717

718 **MIP panel design**

719 A double-stranded DNA MIP panel targeting 1.4 Mb across exons and exon-intron junctions of
720 88 neurodegenerative genes was designed using custom scripts incorporating MIPgen[74] using the
721 human reference genome, hg19, with Mly1 restriction sites masked with 'N' using bedtools. The
722 final panel of 26,439 MIPs captures an average fragment length of 209 bp, including the
723 extension and ligation arms to ensure overlapping of the forward and reverse sequencing read.
724 The panel successfully targets 92.7% of bases including flanking intronic regions, with > 98% of
725 exonic bases covered with an average of at least 2 unique MIPs. All MIPs were designed to
726 include a custom backbone consisting of primer binding sites and dual 5-nt unique molecular
727 identifier (UMI). MIPs were rebalanced in the pool based on the percent of GC content within
728 the regions to improve coverage at GC-rich regions. We increased the copied MIPs that bind to
729 GC-rich regions with the following criteria: 60-70% GC = 2 copies; 70-80% GC = 5 copies; 80-
730 90% GC = 8 copies; > 90% GC = 10 copies. Common primer binding and Mly1 restriction
731 enzyme sites were added to both ends of the oligo sequences to enable blunt-end removal of the
732 primer binding sites. The forward and reverse compliment sequences were printed into a single
733 ssDNA pool by CustomArray (Bothell, WA). The resulting panel was amplified at a low cycle
734 number (12×), digested with Mly1 enzyme for 12 h at 37 °C, and purified using Qiagen
735 Nucleotide removal kit.
736

737 **MIP capture and library construction**

738 Two hundred fifty ng of gDNA was first hybridized in a 15 µl reaction with 1.5 µl of
739 Ampligase® 10× Reaction Buffer (VWR), 1.5 µl of the reverse blocking oligo (5'-
740 NNNNGAAGTCGAAGGGCTATAGGCTGCCATCACANNNN-3') and the MIP pool at 63
741 nM for 10 min at 95 °C and 24 h at 60 °C. Gap-fill/ligation was then performed by adding 1 unit
742 of Phusion™ High-Fidelity DNA Polymerase (Thermo Fisher), 4 units of Ampligase® DNA
743 Ligase (Epicentre), 0.2 µl of Ampligase® 10× Reaction Buffer, 0.6 µl of dNTPs (10 mM) and 1
744 µl of nuclease-free water to the MIP capture product and incubated at 60 °C for 1 h. For
745 exonuclease digestion, 50 units of Exonuclease III (Thermo Fisher), 10 units of Exonuclease I
746 (Thermo Fisher), 0.2 µl of Ampligase® 10× Reaction Buffer (VWR), and 2.05 µl of nuclease-
747 free water was added to the Gap-fill/ligation product, which was incubated for 40 min at 37 °C
748 and 5 min at 95 °C. Ten µl of the captured library is amplified in a 50 µl final reaction by adding
749 1 unit of Phusion Hot Start II DNA Polymerase (Thermo Fisher), 10 µl of 5× HF buffer, 1 µl of

750 dNTPs (10mM), 1 µl of the universal MIP barcode forward primer (10 µM), 1 µl of the
751 individual barcode reserve primer (10 µM) and 26.5 µl of nuclease-free water. MIP library
752 amplification was then performed under the following conditions: 98 °C for 30 s; 16 cycles of
753 98 °C for 10 s, 60 °C for 30 s and 72 °C for 30 s; 72 °C for 2 min. MIP library was then purified
754 using 2× AMPure XP Beads (Beckman Coulter,) and quantified by the Quant-iT™ dsDNA
755 Assay HS Kit (Thermo Fisher). Ninety-six MIP libraries were pooled together and sequenced on
756 one lane of Illumina Hiseq X.
757
758 **Pre-processing and read mapping of MIP sequencing data**
759 MIP sequencing primers were removed first from the raw FASTQ files using Cutadapt[75] (v2.4;
760 5' adapter of the first read: CATACGAGATCCGTAATCGGGAAGCTGAAG; 3' adapter of the
761 first read: ACACTACCGTCGGATCGTGCGTGT; 5' adapter of the second read:
762 GCTAAGGGCCTAACTGGCCGCTTCACTG; 3' adapter of the second read:
763 CTTCAGCTTCCCGATTACGGATCTCGTATG). Trimmed reads were aligned to the human
764 reference genome (GRCh37) using BWA-mem[76] (v0.7.15) and sorting and indexing were
765 performed using samtools[77] (v1.3.1). From the aligned BAM file, off-target reads were removed
766 by checking the overlaps with the target regions using bedtools[78] (v2.26.0). MIP arm regions
767 were masked by soft-clipping for each read using BAMClipper[79] (v1.0.1). UMI information was
768 extracted, and then mapped reads were deduplicated based on the mapping coordinate and the
769 shared UMI using UMI-tools[80] (v1.0.0). Base quality score recalibration and local realignment
770 were performed using the Genome Analysis Toolkit (GATK, v3.7)[81], generating final analysis-
771 ready BAMs.
772
773 **Variant calling for germline variants**
774 Initial candidates of germline SNVs and indels were identified using GATK HaplotypeCaller
775 with default parameter settings. Low-quality candidates were filtered out if any of the following
776 conditions is not satisfied: (1) ≥ 10 variant-supporting reads; (2) ≥ 20 total read-depth at the
777 variant site; (3) VAF ≥ 0.3; (4) GATK QUAL ≥ 50, and; (5) identified in all brain regions from
778 the same individual except for the samples failed to cover the variant site (<10 reads). Possible
779 pathogenic germline variants were further selected by satisfying all the following conditions: (1)
780 present in less than 0.1% of the population in any ancestry group of public databases including
781 dbSNP[82], the 1000 Genomes Project[83], the Exome Aggregation Consortium (ExAC)[84], the
782 Genome Aggregation Database (gnomAD)[85], the NHLBI Exome Sequencing Project
783 (ESP6500)[86], the Greater Middle East variome project (GME)[87], and Kaviar database[88]; (2)
784 candidates observed only in disease or control groups but not in both; (3) possible protein-
785 altering candidates (missense, nonsense, frame-shift, or splicing variants), and; (4) affecting 30
786 ALS- and FTD-related genes. Deleteriousness prediction module (see computational prediction
787 of variant deleteriousness section below) was then applied to the remaining candidates, and
788 predicted deleterious variants were reported as final deleterious germline variants. ANNOVAR[26]
789 was used to annotate the genomic region, affected genes, population allele frequency, and exonic
790 variant functions. SpliceAI[89] was additionally utilized to identify more splice-altering variants.
791 Candidates with delta score > 0.5 were considered to be possible splicing variants.
792
793 **Repeat-primed PCR assay for *C9orf72* repeat expansion genotyping**
794 Repeat-primed PCR (RP-PCR) of the *C9orf72* repeat expansion was performed in a 30 µl PCR
795 reaction with 150 ng of gDNA, 15 µl of 2× FastStart™ PCR Master (Roche), 2 µl of DMSO, 5 µl

796 of 5× Q-solution (Qiagen), 1 µl of 5 mM 7-deaza-dGTP (NEB), 1 µl of 25 mM $MgCl_2$ (Qiagen)
797 and 1 µl of the primer mix (40 µM of the Forward primer: 5'-/56-
798 FAM/AGTCGCTAGAGGCGAAAGC-3'; 20 µM of the Reverse primer: 5'-
799 TACGCATCCCAGTTTGAGACGGGGGCCGGGGCCGGGGCCGGGG-3'; 40 µM of the
800 Anchor/tail primer: 5'-TACGCATCCCAGTTTGAGACG-3'). The reaction was performed with
801 touchdown PCR cycling conditions consisting of 15 min at 95 °C, followed by cycles of 94 °C
802 for 1 min, annealing starting at 70 °C for 1 min, and extension at 72 °C for 3 min, ending with a
803 final extension step of 10 min at 72 °C. The annealing temperature was decreased in 2 °C steps
804 as follows: 70 °C for two cycles, 68 °C for three cycles, 66 °C for four cycles, 64 °C for five
805 cycles, 62 °C for six cycles, 60 °C for seven cycles, 58 °C for eight cycles, and 56 °C for five
806 cycles. The RP-PCR products were separated by the SeqStudio Genetic Analyzer (Thermo
807 Fisher) with the GeneScan™ 600 LIZ™ Dye Size Standard (Thermo Fisher). Results of
808 fragment sizes were analyzed by Peak Scanner™ Software v1.0 (Thermo Fisher).
809
810 **Somatic variant calling from MIP sequencing data**
811 Three different callers RePlow (v1.1.0)[38], Mutect2 (v4.1.5)[39], and Pisces (v5.2.11)[40] were used to
812 generate initial candidate sets. RePlow is optimized for detecting low-VAF somatic variants
813 from deep targeted sequencing data. It generates a profile of background errors per substitution
814 type and utilizes these distributions as priors in a Bayesian model to estimate the probability of a
815 variant candidate being an error. MuTect2 is one of the most widely used somatic variant callers,
816 particularly sensitive to detecting low-VAF variants in impure and heterogeneous samples. It
817 employs a Bayesian classifier to evaluate the likelihood of a variant being genuine versus a
818 sequencing error and applies multiple filters to reduce false positives. Pisces is specifically
819 designed for detecting somatic mutations from amplicon sequencing data, particularly in cases
820 where no matched control sample is available. It stitches paired-end reads into consensus reads
821 and recalibrates variant quality scores specifically tuned to address amplification-related errors
822 such as thermal damage or deamination, often observed in FFPE samples.
823 Each sample was analyzed by all three callers using single-sample mode. Default
824 parameter settings were used except for the adjustments for disabling the coverage limit.
825 Variants that passed all the filters from each caller were used to make three different initial sets.
826 Candidates identified by only one caller were discarded, and those called at least two callers
827 were retained as a double-call set. For indels, double-calls between Mutect2 and Pisces were
828 used as somatic indel candidates since RePlow does not support indel detection. For SNVs,
829 among double-calls Mutect2-Pisces pairs were additionally filtered out due to high false positive
830 rates and low validation rates in the benchmarking data set (Extended Data Fig. 3d). Remaining
831 RePlow-based SNV double-calls and indel candidates were subject to multi-step variant filters to
832 further remove false positive candidates.
833 Unlike germline variant calling, somatic variant calling aims to reliably detect low-VAF
834 variants up to ~0.5%, which requires enough supporting evidence to control the false positive
835 rate. Calling thresholds such as variant-supporting read count, read-depth at the variant site, and
836 average base-call quality were determined based on the benchmarking data. Somatic variants
837 were selected satisfying all the following conditions: (1) ≥ 50 total read-depth at the variant site;
838 (2) ≥ 15 variant-supporting reads excluding the reads with the variant allele on their probe-arm
839 regions; (3) > 30 average base-call quality of variant allele; (4) ≥ 2 different types of variant-
840 supporting amplicons; (5) $0.001 \leq VAF \leq 0.4$; (6) ≤ 3 variant candidates within 20-bp window

841 from the same sample; (7) present in less than 0.1% of the population in any ancestry group of
842 public databases, and; (8) observed in no more than two different individuals.
843 Somatic variants were further annotated with similar criteria for selecting predicted
844 deleterious germline variants. Among the final candidates, variants that are (1) observed only in
845 disease or control groups but not in both, (2) possible protein-altering variants, and (3) affecting
846 ALS- and FTD-related genes were selected and applied for the deleteriousness prediction
847 module. ANNOVAR and SpliceAI were utilized to annotate variants with various genomic
848 information and detect additional splice-altering variants, respectively.
849
850 **Computational prediction of variant deleteriousness**
851 Deleteriousness prediction module was applied to filtered germline and somatic variants to refine
852 the predicted deleterious (potentially pathogenic) candidate sets. Variants that were previously
853 reported as benign/likely benign in the clinical databases (ClinVar[90] and Human Gene Mutation
854 Database[91]) were excluded from the predicted candidate set. Nonsense, frameshift, and
855 canonical splicing variants (±1-2 splice sites) were assumed to disrupt gene function and were
856 included in the predicted deleterious set. For missense variants, the dbNSFP database[92] was
857 utilized to adopt multiple computational algorithms (SIFT[93], PolyPhen2[94], LRT[95],
858 MutationTaster[96], MutationAssessor[97], FATHMM[98], FATHMM-MKL[99], PROVEAN[100],
859 MetaSVM[101], MetaLR[101]), considering damaging effects at different levels such as biochemical
860 property, protein structure, and evolutionary conservation. Categorical prediction results of each
861 algorithm were delivered by ANNOVAR. A missense variant was selected to be predicted
862 deleterious if at least three different algorithms predicted damaging effects (deleterious for SIFT,
863 LRT, FATHMM, PROVEAN, MetaSVM and MetaLR; probably damaging for PolyPhen2;
864 disease-causing for MutationTaster). Possibly/likely damaging predictions were excluded for
865 more conservative selection. For ALS/FTD-related genes, previously reported inheritance
866 patterns (dominant/recessive) were carefully checked. For recessive genes, two independent
867 variants in the same gene were required to determine whether a given individual was affected by
868 predicted deleterious variants.
869
870 **Benchmarking with spike-in datasets**
871 Extracted gDNA from two Coriell cell lines (GM12878 and GM24695) were used to generate a
872 spike-in data. Extracted DNA were mixed at five different levels to mimic low-level somatic
873 variants, targeting the VAFs of 0.5%, 1%, 2.5%, 5%, and 10%. Genomic DNA from GM12878
874 cells was spiked into DNA from GM24695, therefore unique germline SNPs in GM12878 were
875 served as somatic variants. Genomic position and genotype information for germline SNPs of
876 Coriell samples were obtained from NIST high-confidence call sets[102]. A total of 165 SNPs (57
877 homozygous and 108 heterozygous SNPs) were initially covered by our designed MIP panel.
878 Among them, we only utilized heterozygous SNPs for benchmarking to accurately reflect target
879 VAFs. Additionally, we excluded the spike-in variants from benchmarking if (1) a given site
880 could be covered by only one amplicon, or (2) have read-depth of less than 100, as these are low-
881 quality variants unable to be detected due to inherent issues with panel design rather than the
882 variant calling process. RePlow, Mutect2, Pisces, and their combinations were tested. Detected
883 variants not in the benchmark set were considered to be false positives, except for GM24695
884 germline SNPs and excluded spike-in variants.
885
886 **Somatic variant calling from bulk RNA-seq data**

887 Raw bam files of bulk RNA-seq and matched WGS data for sALS and control cases of the New
888 York Genome Center ALS Consortium were obtained from the New York Genome Center.
889 RNA-seq reads extracted from raw bam files were aligned to the GRCh38 human reference
890 genome by STAR (v2.5.0a)[103] in the two-pass mode with the reference gene annotation
891 (Gencode version 39). The aligned bam files were processed by Picard (v1.138) to remove
892 duplicates, and then by GATK (v3.6)[104] for SplitNCigarReads, indel realignment, and base
893 quality recalibration. We further excluded reads that were improperly paired or with ambiguous
894 alignment.
895 Somatic SNVs were called by RNA-MosaicHunter (v1.0) with default parameters.
896 Derived from MosaicHunter[105], which was designed for somatic variant calling in DNA
897 sequencing, RNA-MosaicHunter incorporates a Bayesian genotyper and a series of empirical
898 filters to systematically distinguish somatic variants from technical artifacts and germline
899 variants, with 59% sensitivity and 94% precision benchmarked using cancer datasets.
900 Specifically, germline variants identified from the matched WGS data from the same individual
901 were excluded. We excluded A-to-G candidates because they are most likely led by the
902 widespread A-to-I(G) RNA editing events in the human genome. To remove recurrent artifacts,
903 we only considered exonic candidates that were called in one or two individuals. We further
904 excluded candidates present in human polymorphism databases including dbSNP[82], the 1000
905 Genomes Project[106], the Exome Sequencing Project[107], and the Exome Aggregation
906 Consortium[108].
907
908 **Long-read targeted sequencing**
909 The PureTarget kit (PacBio) was used to prepare sequencing libraries with 2 µg of high-
910 molecular-weight DNA following the manufacturer's protocol. Pooled libraries were sequenced
911 on one Revio SMRT Cell. Raw HiFi reads were aligned to the human reference genome
912 (GRCh38) using minimap2 (v2.28)[109], and sorting and indexing were performed using samtools
913 (v1.3.1)[77]. The Tandem Repeat Genotyping Tool (TRGT, v1.1.1)[110] was used to determine the
914 *C9orf72* repeat counts for each sample (chr9:27573528-27573546, (GGGGCC)n). A waterfall
915 plot was generated using TRVZ to visualize repeat counts with mosaicism.
916
917 **Nuclei isolation and whole genome amplification**
918 Isolation of total (DAPI+), neuronal (NeuN+), non-neuronal (NeuN-), and damaged (low DAPI)
919 nuclei were achieved by FANS together with nuclear staining of NeuN (Millipore, MAB377,
920 clone A60, 1:1,500) and DAPI following a previously published study[111]. Five hundred nuclei of
921 each cell population were sorted into wells of 96-well plates.
922 Sorted nuclei were subjected to genome amplification using the Primary Template-
923 directed Amplification kit (BioSkryb, 100136) following the manufacturer's protocol.
924
925 **Amplicon sequencing**
926 Primer sets targeting each identified somatic SNV were designed using BatchPrimer3
927 (Supplementary Table 11). Amplicon was amplified for 25 cycles in a 50 µl PCR reaction with
928 50 ng of gDNA, 1 unit of Phusion Hot Start II DNA Polymerase (Thermo Fisher), 10 µl of 5×
929 HF buffer, 1 µl of dNTPs (10 mM) and 10 µl of each primer (10 µM). Amplicon PCR products
930 were then purified by a 0.65× + 1.05× double size selection with AMPure XP Beads (Beckman
931 Coulter, A63882). Purified amplicons were then pooled based on the concentrations measured by

932 the Quant-iT™ dsDNA Assay HS Kit (Thermo Fisher) and sequenced using Amplicon-EZ
933 (Genewiz).
934
935 **Immunohistochemistry**
936 Immunohistochemistry was performed using DAB (3,3'-Diaminobenzidine) detection following
937 published protocols[112]. Briefly, 7-µm formalin-fixed, paraffin-embedded (FFPE) sections were
938 dewaxed using citrisolve, before being rehydrated through decreasing concentrations of ethanol.
939 Antigen retrieval was performed using sodium citrate buffer pH 6.0 at 121 °C for 15 min.
940 Endogenous peroxidases were blocked using 3% hydrogen peroxide solution, and non-specific
941 binding was blocked using 10% normal goat serum. Sections were then incubated overnight at
942 4 °C with primary antibody (pTDP-43 mouse polyclonal, CosmoBio CAC-TIP-PTD-P03,
943 1:10,000). After washing with TBS-Triton, sections were incubated with a Horseradish
944 peroxidase (HRP)-conjugated Goat anti-mouse secondary (Dako) for 1 h at room temperature.
945 HRP signal was detected using DAB substrate (Dako) applied for 15 min. Counterstaining was
946 performed using Coles hematoxylin for 1 min. Sections were then dehydrated, cleared using
947 citrisolve, and mounted using glass coverslips. All sections were viewed using a Leica upright
948 light microscope and assessed for section quality prior to whole-slide digital scanning.
949
950 **Quantification of p-TDP43 burden by immunohistochemistry**
951 Stained sections were scanned using a NanoZoomer whole-slide digital imager at 40X
952 magnification. Images were then visualized and quantified using QuPath image analysis software
953 and algorithms following published protocols[112]. Briefly, for cortical/cerebellar sections 5 ROI
954 measuring 3 mm^2 (1000 × 3000 µm) were placed equidistantly around a single gyrus with the
955 short end of the ROI placed at the pial surface. Pathology was then quantified using a positive
956 pixel count within each ROI and measurements were averaged to provide an output of positive
957 pixels/mm^2. For spinal cord sections, square ROI (2.25 mm^2) was placed on each side of the
958 central canal within the anterior horn and measurements were averaged.
959
960 **Data Availability**
961 The bulk RNA-seq data generated by the NYGC ALS Consortium are available through
962 controlled access via the Target ALS Data Portal (https://dataengine.targetals.org/). Access
963 requires acceptance of the Target ALS Data Use Agreement and submission of a data access
964 request through the portal application process. Additional details are provided in the Target ALS
965 Data Portal User Manual. The MIP-based targeted sequencing data and long-read sequencing
966 data generated in this study have been deposited in dbGaP under accession number phs003530,
967 with access governed by human subject privacy regulations. Germline and somatic variants
968 identified and validated in this study are listed in the supplementary tables.
969
970 **Code Availability**
971 The source code and default configuration file of RNA-MosaicHunter have been published and
972 are available at https://github.com/AugustHuang/RNA-MosaicHunter. Other custom analysis
973 scripts used in this study are publicly available at GitHub (https://github.com/kimjh607/ALS-
974 FTD-somatic-mosaicism) and archived at Zenodo (https://doi.org/10.5281/zenodo.18682277).
975

Methods-only References

74. Boyle, E. A., O'Roak, B. J., Martin, B. K., Kumar, A. & Shendure, J. MIPgen: optimized modeling and design of molecular inversion probes for targeted resequencing. *Bioinformatics* **30**, 2670-2672 (2014).
75. Martin, M. Cutadapt removes adapter sequences from high-throughput sequencing reads. *2011* **17**, 3 (2011).
76. Li, H. Aligning sequence reads, clone sequences and assembly contigs with BWA-MEM. *arXiv preprint arXiv:1303.3997* (2013).
77. Danecek, P. *et al.* Twelve years of SAMtools and BCFtools. *Gigascience* **10**, giab008 (2021).
78. Quinlan, A. R. & Hall, I. M. BEDTools: a flexible suite of utilities for comparing genomic features. *Bioinformatics* **26**, 841-842 (2010).
79. Au, C. H., Ho, D. N., Kwong, A., Chan, T. L. & Ma, E. S. K. BAMClipper: removing primers from alignments to minimize false-negative mutations in amplicon next-generation sequencing. *Sci. Rep.* **7**, 1567 (2017).
80. Smith, T., Heger, A. & Sudbery, I. UMI-tools: modeling sequencing errors in Unique Molecular Identifiers to improve quantification accuracy. *Genome Res.* **27**, 491-499 (2017).
81. Van der Auwera, G. A. *et al.* From FastQ data to high confidence variant calls: the Genome Analysis Toolkit best practices pipeline. *Curr. Protoc. Bioinformatics* **43**, 11.10.1-11.10.33 (2013).
82. Sherry, S. T. *et al.* dbSNP: the NCBI database of genetic variation. *Nucleic Acids Res.* **29**, 308-11 (2001).
83. 1000 Genomes Project Consortium *et al.* A global reference for human genetic variation. *Nature* **526**, 68-74 (2015).
84. Karczewski, K. J. *et al.* The ExAC browser: displaying reference data information from over 60 000 exomes. *Nucleic Acids Res.* **45**, D840-D845 (2017).
85. Karczewski, K. J. *et al.* The mutational constraint spectrum quantified from variation in 141,456 humans. *Nature* **581**, 434-443 (2020).
86. Fu, W. *et al.* Analysis of 6,515 exomes reveals the recent origin of most human protein-coding variants. *Nature* **493**, 216-20 (2013).
87. Scott, E. M. *et al.* Characterization of Greater Middle Eastern genetic variation for enhanced disease gene discovery. *Nat. Genet.* **48**, 1071-1076 (2016).
88. Glusman, G., Caballero, J., Mauldin, D. E., Hood, L. & Roach, J. C. Kaviar: an accessible system for testing SNV novelty. *Bioinformatics* **27**, 3216-3217 (2011).
89. Jaganathan, K. *et al.* Predicting splicing from primary sequence with deep learning. *Cell* **176**, 535-548.e24 (2019).
90. Landrum, M. J. *et al.* ClinVar: improving access to variant interpretations and supporting evidence. *Nucleic Acids Res.* **46**, D1062-D1067 (2018).
91. Stenson, P. D. *et al.* Human Gene Mutation Database (HGMD): 2003 update. *Hum. Mutat.* **21**, 577-581 (2003).
92. Liu, X., Wu, C., Li, C. & Boerwinkle, E. dbNSFP v3.0: a one-stop database of functional predictions and annotations for human nonsynonymous and splice-site SNVs. *Hum. Mutat.* **37**, 235-41 (2016).
93. Kumar, P., Henikoff, S. & Ng, P. C. Predicting the effects of coding non-synonymous variants on protein function using the SIFT algorithm. *Nat. Protoc.* **4**, 1073-1081 (2009).

1022 94. Adzhubei, I. A. *et al.* A method and server for predicting damaging missense mutations.
1023 *Nat Methods* **7**, 248-249 (2010).
1024 95. Chun, S. & Fay, J. C. Identification of deleterious mutations within three human
1025 genomes. *Genome Res.* **19**, 1553-1561 (2009).
1026 96. Schwarz, J. M., Rodelsperger, C., Schuelke, M. & Seelow, D. MutationTaster evaluates
1027 disease-causing potential of sequence alterations. *Nat. Methods* **7**, 575-576 (2010).
1028 97. Reva, B., Antipin, Y. & Sander, C. Predicting the functional impact of protein mutations:
1029 application to cancer genomics. *Nucleic Acids Res.* **39**, e118 (2011).
1030 98. Shihab, H. A. *et al.* Predicting the functional, molecular, and phenotypic consequences of
1031 amino acid substitutions using hidden Markov models. *Hum. Mutat.* **34**, 57-65 (2013).
1032 99. Shihab, H. A. *et al.* An integrative approach to predicting the functional effects of non-
1033 coding and coding sequence variation. *Bioinformatics* **31**, 1536-1543 (2015).
1034 100. Choi, Y., Sims, G. E., Murphy, S., Miller, J. R. & Chan, A. P. Predicting the functional
1035 effect of amino acid substitutions and indels. *PLoS One* **7**, e46688 (2012).
1036 101. Dong, C. *et al.* Comparison and integration of deleteriousness prediction methods for
1037 nonsynonymous SNVs in whole exome sequencing studies. *Hum. Mol. Genet.* **24**, 2125-
1038 2137 (2015).
1039 102. Zook, J. M. *et al.* Integrating human sequence data sets provides a resource of benchmark
1040 SNP and indel genotype calls. *Nat. Biotechnol.* **32**, 246-251 (2014).
1041 103. Dobin, A. *et al.* STAR: ultrafast universal RNA-seq aligner. *Bioinformatics* **29**, 15-21
1042 (2013).
1043 104. DePristo, M. A. *et al.* A framework for variation discovery and genotyping using next-
1044 generation DNA sequencing data. *Nat. Genet.* **43**, 491-498 (2011).
1045 105. Huang, A. Y. *et al.* MosaicHunter: accurate detection of postzygotic single-nucleotide
1046 mosaicism through next-generation sequencing of unpaired, trio, and paired samples.
1047 *Nucleic Acids Res.* **45**, e76 (2017).
1048 106. 1000 Genomes Project Consortium *et al.* An integrated map of genetic variation from
1049 1,092 human genomes. *Nature* **491**, 56-65 (2012).
1050 107. Tennessen, J. A. *et al.* Evolution and functional impact of rare coding variation from deep
1051 sequencing of human exomes. *Science* **337**, 64-69 (2012).
1052 108. Lek, M. *et al.* Analysis of protein-coding genetic variation in 60,706 humans. *Nature*
1053 **536**, 285-291 (2016).
1054 109. Li, H. Minimap2: pairwise alignment for nucleotide sequences. *Bioinformatics* **34**, 3094-
1055 3100 (2018).
1056 110. Dolzhenko, E. *et al.* Characterization and visualization of tandem repeats at genome
1057 scale. *Nat. Biotechnol.* **42**, 1606-1614 (2024).
1058 111. Evrony, G. D. *et al.* Single-neuron sequencing analysis of L1 retrotransposition and
1059 somatic mutation in the human brain. *Cell* **151**, 483-496 (2012).
1060 112. Nolan, M. *et al.* Quantitative patterns of motor cortex proteinopathy across ALS
1061 genotypes. *Acta Neuropathol Commun* **8**, 98 (2020).
1062